Follicle cell contact maintains main body axis polarity in the *Drosophila melanogaster* oocyte

Ana Milas, Jorge de-Carvalho and Ivo A. Telley

Instituto Gulbenkian de Ciência, Rua da Quinta Grande 6, 2780-156 Oeiras, Portugal

Correspondence: Ivo A. Telley (itelley@igc.gulbenkian.pt)

Keywords: Par protein, symmetry break, oogenesis, cytoskeletal polarity, Drosophila

Abstract

In *Drosophila melanogaster* the anterior-posterior body axis is maternally established and governed by differential localization of partitioning defective (Par) proteins within the oocyte. At mid-oogenesis, Par-1 accumulates at the posterior end of the oocyte while Par-3/Bazooka is excluded there but maintains its localization along the remaining oocyte cortex. This mutual exclusion leads to a polarized microtubule network and accumulation of posterior determinant *oskar* later in oogenesis. Reciprocal biochemical interactions between Par proteins can explain their cortical exclusion and domain formation – for example, Par-1 excludes Par-3 by phosphorylation. However, past studies have proposed the need for somatic cells at the posterior end to initiate oocyte polarization by providing a trigger signal. To date, despite modern screening approaches and genetic manipulation, neither the molecular identity nor the nature of the signal is known. Here, we provide the first evidence that mechanical contact of posterior follicle cells (PFCs) with the oocyte cortex causes the posterior exclusion of Bazooka and maintains oocyte polarity. We show that Bazooka prematurely accumulates exclusively where posterior follicle cells have been mechanically detached or ablated. This occurs before Par-1 is removed suggesting that phosphorylation of Bazooka by Par-1 is not sufficient to maintain Bazooka exclusion in the absence of PFC contact. Furthermore, we provide evidence that PFC contact maintains Par-1 and *oskar* localization and microtubule cytoskeleton polarity in the oocyte. Our observations suggest that cell-cell contact mechanics modulates Par protein binding sites at the oocyte cortex.

Introduction

A large majority of animals form two embryonic body axes (Niers, 2010). In many animals, these body axes are formed after fertilization, during early embryonic growth and segmentation. In *Drosophila melanogaster*, the anterior-posterior axis is maternally established, gradually during 14 stages of oogenesis, with the final goal of delivering *oskar* mRNA to the posterior end and *bicoid* mRNA to the anterior end of the oocyte (Riechmann and Ephrussi, 2001). The first sign of anterior-posterior polarity is the positioning of the oocyte to the posterior of the egg chamber at stage 1, which is achieved through differential adhesion between the oocyte and the somatic cells at the posterior of the egg chamber (Godt and Tepass, 1998; González-Reyes and St Johnston, 1998).

At stage 6, the posteriorly positioned oocyte secrets the EGF-like ligand, Gurken, which will cause the subset of follicle cells at the posterior to adopt posterior fate. In the following stage, these posterior follicle cells (PFCs) will signal back to the oocyte to determine its posterior pole (González-Reyes and St Johnston, 1994; González-Reyes et al., 1995; Roth et al., 1995). However, the molecular nature of the signal coming back from the PFCs remains elusive. Additionally, it is unclear if this signal acts solely as trigger that breaks symmetry, or if PFCs play a role in maintenance of oocyte polarity.

The earliest known signature of mid-stage oocyte polarization following the signal from PFCs is the di-phosphorylation of non-muscle Myosin II at the posterior of the oocyte (Doerflinger et al., 2022). This is necessary for posterior localization of Par-1 kinase, which is a component of a highly conserved network of Partitioning defective (Par) proteins (Shulman et al., 2000; Tomancak et al., 2000). Following Par-1 localization to the posterior, the anterior group of Par proteins, including aPKC, Par-6 and Par-3/Bazooka, relocalizes from the posterior to the anterolateral cortex (Doerflinger et al., 2010; Jouette et al., 2019). Posteriorly localized Par-1 inhibits nucleation of microtubules, causing plus ends of microtubules to preferentially accumulate at the posterior (Nashchekin et al., 2016; Parton et al., 2011). Polarization of the microtubule network is necessary to direct kinesin-dependent transport of *oskar* mRNA to the posterior during stages 9 and 10A (Lu et al., 2018, 2020; Zimyanin et al., 2008). Therefore, it is crucial that the polarity of the Par network is maintained during these stages.

The asymmetry of the Par network is thought to be self-maintaining through mutual antagonism between anterior and posterior Par proteins (Hoege and Hyman, 2013; Lang and Munro, 2017; Motegi and Seydoux, 2013). Par-1 phosphorylates Bazooka to exclude the complex of aPKC/Par-6/Bazooka from the posterior, while aPKC phosphorylates Par-1 leading to the removal of Par-1 from the anterolateral membrane (Benton and St Johnston, 2003a; Doerflinger et al., 2010). Interestingly, anterior and posterior Par proteins colocalize at the posterior of the oocyte from stage 7 to stage 9, suggesting that mutual antagonism might not be sufficient to maintain Par polarity (Doerflinger et al., 2010; Jouette et al., 2019).

61 Here, we first show that at late stage 10B of oogenesis the cell-cell interface of the oocyte and PFCs
62 visibly enlarges, suggesting contact loss, followed by accumulation of Bazooka and removal of Par-1 at
63 the posterior of the oocyte. Mechanical detachment of PFCs from the oocyte at stage 9 and 10A by
64 micromanipulation causes loss of contact and premature accumulation of Bazooka. The exclusion of
65 Bazooka from the posterior is rapidly reverted following laser ablation of PFCs. Bazooka accumulates at
66 the posterior before Par-1 is removed, suggesting that Par-1 phosphorylation of Bazooka is not sufficient
67 to maintain Bazooka exclusion once PFC contact is lost. Following PFC ablation, Par-1 delocalizes slowly
68 leading to loss of *oskar* mRNA localization at the posterior, but this occurs faster than the rate at which
69 Par-1 targeting kinase aPKC accumulates. Finally, microtubules polymerize at the posterior, but after
70 *oskar* delocalizes. We conclude that PFCs maintain polarity of the Par network by cell-cell contact until
71 late stage 10B of oogenesis by excluding Bazooka from the posterior of the oocyte. This is necessary to
72 anchor *oskar* mRNA at the posterior, and to maintain polarization of the microtubule network during
73 stages at which *oskar* is delivered to the posterior by directed transport.

74 **Results**

75 **Posterior relocalization of Bazooka following contact loss with PFCs in stage 10B oocytes**

76 The localization patterns of Bazooka have been well described up until early stage 10 of oogenesis. At
77 stages 7 and 8, Bazooka localizes to the posterior of the oocyte, where it overlaps with the Par-1 domain,
78 until stage 9 when it is excluded from the posterior (Doerflinger et al., 2010; Jouette et al., 2019).
79 However, the dynamics of Bazooka localization in the following stages is not known. To assess this, we
80 performed live cell imaging of stage 10 and 11 egg chambers expressing Bazooka tagged with GFP
81 (Baz::GFP) and Jupiter tagged with mCherry (Jupiter::mCherry) as a reporter for microtubules (Fig. 1).
82 We used the GAL4/UASp system to express Bazooka only in the germline, since Bazooka localizes to the
83 apical side of follicle cells, thus masking the localization of Bazooka at the oocyte membrane (Jouette et
84 al., 2019). In agreement with previous results, all but one oocyte show exclusion of Bazooka at stage 10A
85 (n=13). More interestingly, the oocyte is tightly connected to the PFCs at this stage, i.e., a clear cellular
86 boundary between the oocyte and the PFCs is not detected in fluorescence confocal images of
87 microtubules and in polarized transmission light microscopy images (Suppl. Fig. 1A, arrowheads). On the
88 other hand, there is a visible gap between the lateral follicle cells and the oocyte. This differential contact
89 correlated with the accumulation of Bazooka; Bazooka localizes at the membrane where the oocyte is not
90 in contact with the follicle cells and is excluded where the contact is established (Suppl. Fig. 1A). At stage
91 11, the cell-cell contact between the oocyte and the PFCs is lost, and a clear boundary is visible, while the
92 exclusion of Bazooka is lost as well (Suppl. Fig. 1B, arrowhead). To understand if the formation of an
93 intercellular space (gap) between PFCs and the oocytes precedes or follows the accumulation of Bazooka
94 at the posterior, we analyzed stage 10B egg chambers in which this transition likely occurs (Fig. 1A–C).
95 The posterior gap is visible in 83% (30 out of 36) stage 10B egg chambers. However, Bazooka was still

96 excluded from the posterior in 12 of these oocytes (Fig. 1D). Importantly, we did not observe egg
97 chambers where Bazooka accumulated to the posterior before the gap formed. The inter-cellular gap forms
98 first anterolaterally sometime during stage 9, before Bazooka is excluded (Fig. 1D). We conclude that the
99 loss of contact between the oocyte and PFCs precedes accumulation of Bazooka (Fig. 1E).

100 **Bazooka accumulates at the posterior before Par-1 clearance at late stage 10B of oogenesis**

101 In *par1* mutant oocytes Bazooka localizes all around the cortex, suggesting that Par-1 phosphorylates
102 Bazooka to exclude it from the posterior (Benton and St Johnston, 2003a). To assess if Par-1 needs to be
103 removed from the posterior before Bazooka accumulates, we imaged oocytes expressing fluorescently
104 tagged Par-1 and Bazooka. At stage 10A, we found Bazooka exclusion and Par-1 enrichment in all
105 analyzed oocytes (n=12) (Suppl. Fig. 1C–F). On the other hand, at stage 11, differential localization of
106 both Bazooka and Par-1 at the posterior were lost (n=10) (Suppl. Fig. 1E–F). At stage 10B, Bazooka
107 relocalized to the posterior in 25 out of 40 oocytes. However, Par-1 was still present at the posterior in 12
108 of these oocytes (Suppl. Fig. 1D, F). Importantly, we never found Par-1 disappearing from the posterior
109 before accumulation of Bazooka. Therefore, Bazooka first accumulates to the posterior, which eventually
110 leads to the removal of Par-1 from this region. This result suggests that Bazooka accumulation is not the
111 consequence of Par-1 removal, and that Par-1 is not sufficient to exclude Bazooka from the posterior
112 during this transition.

113 Taken together, these observations suggest that the loss of contact between PFCs and the oocyte is
114 followed first by recruitment of Bazooka to the posterior, and only thereafter Par-1 delocalizes from the
115 posterior. We hypothesize that cell-cell contact between PFCs and the oocyte is required to exclude
116 Bazooka from the posterior oocyte membrane.

117 **Mechanical detachment of PFCs from the oocyte causes posterior accumulation of Bazooka.**

118 To directly test the contact interaction between oocyte and PFCs leading to the exclusion of Bazooka, we
119 designed an experiment by which PFCs were mechanically detached from the oocyte. We used a blunt
120 glass micropipette mounted on a micromanipulator to aspirate and pull on the PFCs aiming detachment
121 from the oocyte but keeping them intact (Fig. 2A). We combined this assay with live imaging of egg
122 chambers expressing Baz::GFP in the germline and Jupiter::mCherry in all tissues to observe any changes
123 in polarity in the oocyte (Fig. 2B and Video 1). Indeed, we could observe accumulation of Bazooka to the
124 posterior of the oocyte following detachment of the PFCs (Fig. 2B–C). Importantly, this accumulation was
125 accompanied by the appearance of the intercellular space between oocyte and PFC boundaries (Fig. 2D).
126 We conclude that mechanical pulling on PFCs causes premature intercellular gap formation, which results
127 in the accumulation of Bazooka to the posterior of the oocyte. This suggests that a firm cell-cell
128 interaction between PFCs and the oocyte is important for maintaining Bazooka exclusion at the posterior
129 end of the oocyte.

130 **Posterior follicle cells maintain posterior exclusion of Bazooka with cell size-precision.**

131 Since cell differentiation of follicle cells into PFCs is necessary to establish polarity of the oocyte in the
132 first place, mutants that disrupt their differentiation do not allow testing of their role in polarity
133 maintenance throughout oogenesis. Therefore, we sought of a more acute and spatially targeted
134 perturbation method for disrupting PFCs. We used pulsed UV laser ablation to destroy a small number of
135 PFCs and monitor the resulting changes in Par protein localization in the oocyte, comparing locations
136 where PFCs were removed versus where they are intact. First, we performed ablation in stage 9 or 10A
137 egg chambers that express Baz::GFP in the germline and Jupiter::mCherry in all tissues. In every
138 experiment, Bazooka was excluded from the posterior prior to the ablation (Fig. 3A, t = –1 min). The
139 ablation of a few PFCs resulted in accumulation of Bazooka exclusively to the membrane region facing
140 the ablated cells (Fig. 3B–C and Video 2). Bazooka did not localize at neighboring regions where PFCs
141 were intact (Fig. 3B, arrowheads). A quantification of Baz::GFP intensity along the posterior cortex of the
142 oocyte showed a signal peak confined to the location of ablated PFCs (Fig. 3C, vertical lines). Similar
143 results were obtained when ablated posterior follicle cells did not include the pair of polar cells (Suppl.
144 Fig. 2A–C, Fig. 1E). To account for possible turnover kinetics and photobleaching, we compared
145 Baz::GFP intensity at cortices either facing posterior or facing lateral follicle cells (Fig. 3D, inset),
146 confirming a significant increase and in some experiments a full recovery of Baz::GFP localization at the
147 posterior. A temporal analysis of Baz::GFP intensity after PFC ablation revealed an almost immediate
148 increase (~1 min delay) (Fig. 3E). The accumulation seemed faster and achieved steady state earlier if
149 polar cells were left intact. We generated a spatiotemporal map of average Baz::GFP intensity along the
150 oocyte cortex facing ablated PFCs (Fig. 3F–G). Whenever the ablated region contained the pair of polar
151 cells, Bazooka accumulated in random patches, presumably by being recruited from the cytoplasmic pool
152 (Fig. 3F). In contrast, when the ablated region was flanked by still intact polar cells on one side, and main
153 body follicle cells on the other side, we noticed a signal flow from the anterolateral cortex facing main
154 body follicle cells. However, we did not notice any significant cytoplasmic flow in the time-lapse movies.
155 We concluded that Bazooka predominantly diffused along the membrane from the cortical pool of
156 anterolateral side towards the posterior end.

157 To assure that accumulation of Bazooka is not caused by nonspecific effects of pulsed laser ablation, we
158 performed ablation inside the ooplasm, close to the posterior membrane of the oocyte (Suppl. Fig. 2D and
159 Video 3). We did not observe any accumulation of Bazooka at the oocyte membrane, or around the region
160 that was ablated (Suppl. Fig. 3E–F). We also addressed if ablation of follicle cells may cause nonspecific
161 accumulation of any protein to the membrane. Thus, as additional control experiment, we UV targeted
162 main body (anterolateral) follicle cells in egg chambers expressing Par-1::GFP in the germline and
163 Jupiter::mCherry. At this stage, Par-1 is restricted to the posterior of the oocyte and there is no Par-1
164 signal at the oocyte membrane in contact with main body follicle cells (Suppl. Fig. 3A, left). Importantly,
165 we did not observe any increase in GFP signal following ablation (Suppl. Fig. 3B–C). From all these

166 experiments, we conclude that individual PFCs are required to locally maintain posterior exclusion of
167 Bazooka throughout mid-oogenesis.

168 **Stage dependent maintenance of Par-1 localization by PFCs.**

169 Next, we wanted to test if Par-1 needs to be excluded from the posterior before Bazooka can accumulate,
170 upon ablation of PFCs. According to the mutual exclusion hypothesis of the Par protein network, Par-1
171 presence is responsible for exclusion of the anterior Par protein complex, including Bazooka, through
172 kinase activity (Benton and St Johnston, 2003a). Therefore, we performed the ablation experiments in egg
173 chambers expressing Par-1::GFP and Baz::mCherry in the germline. With this combination of polarity
174 protein reporters, we again observed accumulation of Bazooka to the posterior following the ablation of
175 PFCs (Fig. 4A, Suppl. Fig. 3D and Video 4 and 5). A first analysis suggested that Par-1 does not decrease
176 as rapidly as expected. Ectopic localization of Bazooka was preceded by a rather slow disappearance of
177 Par-1. However, we suspected that the developmental stage marks a difference in Par-1 kinetics upon PFC
178 ablation. In stage 10A oocytes, Par-1 signal marginally decreases within one hour (Suppl. Fig 3F)
179 although longer acquisitions revealed a decrease. In stage 9 oocytes, the signal decrease was more
180 pronounced in the region that had been in contact with ablated PFCs (Fig. 4B–C). Slow signal changes can
181 be either a consequence of late response to the perturbation, or due to photobleaching. Thus, we performed
182 a comparative analysis within each oocyte, and acquired at low light exposure (Methods). Ectopic
183 accumulation of Bazooka at the posterior was significant when compared to the lateral cortex (Fig. 4D),
184 while the Par-1 signal decrease was not significant in stage 10A (Fig. 4E). We conclude that Par-1 is not
185 sufficient to keep Bazooka excluded from the posterior after PFC ablation. Moreover, Par-1 localization is
186 controlled by PFCs in a stage dependent manner.

187 We noticed that Par-1 loss seemed to start in the center of the cortex region which lost contact with PFCs
188 (Suppl. Fig. 3E, arrowhead), and extended towards the cortical boundaries facing intact PFCs. To obtain
189 better insight, we generated a spatiotemporal map of Par-1::GFP intensity along the oocyte cortex facing
190 the ablated PFCs (Fig. 4F). This analysis confirmed a progressive signal loss that occurs symmetrically
191 around the ablation center. In an effort to decompose cortical mobility and turnover kinetics of Par-1::GFP
192 at the posterior cortex, we performed FRAP analysis in the absence of perturbation. Typical Par-1::GFP
193 recovery time was <1 min (Fig. 4G), which contrasts the slow Par-1 delocalization after perturbation,
194 occurring typically within one hour (Fig. 4F). We did not notice any cytoplasmic flow which could
195 potentially transport Par-1 to the boundaries by advection (Video 4 and 5). Thus, our interpretation is that
196 the molecular binding sites for Par-1, which are abundant and cause Par-1 accumulation, slowly delocalize
197 upon PFC ablation while Par-1 turns over fast. Importantly, the spatial signature of delocalization is
198 neither uniform nor random; having excluded advection, it is reminiscent of diffusible binding sites whose
199 mobility within the membrane is reduced when the cortex is in contact with PFCs ("modulated molecular
200 trap").

201 **Posterior *oskar* mRNA is lost upon PFC ablation**

202 A downstream process of Par polarity in the oocyte is *oskar* mRNA accumulation at the posterior, which
203 ultimately defines the tail of the future organism (Riechmann and Ephrussi, 2001). This is achieved by
204 directed transport on a slightly polarized microtubule network and anchoring at the posterior cortex (Lu et
205 al., 2018, 2020; Zimyanin et al., 2008). We wanted to understand if the response of Par proteins to PFC
206 ablation would also affect *oskar* localization. To this end, we performed live cell imaging of stage 8–10A
207 egg chambers expressing Par-1::GFP and *osk*MS2 under its native driver together with MCP::mCherry
208 (Fig. 5A, Video 6). Upon PFC ablation, Par-1 delocalizes slowly, as shown previously (Fig. 5B, top).
209 More strikingly, *oskar* also delocalizes, first in the region previously in contact with ablated PFCs, and
210 gradually also at the flanking regions (Fig. 5B, bottom). Qualitatively, *oskar* delocalization seemed
211 delayed and slower for later stages. An analysis of the signal kinetics for both Par-1 and *oskar* by fitting
212 single exponential decay functions with delay confirmed this impression (Fig. 5C). *oskar* delocalization
213 occurred with a statistically significant delay relative to Par-1. In stage 8 oocytes the overall delocalization
214 kinetics was in the minutes range, while in stage 10A, in particular for *oskar*, the delay and kinetics were
215 in the hour range. We conclude that PFCs are required to maintain body axis definition in the oocyte until
216 stage 10 by defining *oskar* mRNA localization through Par-1.

217 Finally, motivated by earlier reports of Par-1 being a microtubule nucleation inhibitor (Doerflinger et al.,
218 2010; Nashchekin et al., 2016; Parton et al., 2011), we predicted that the delocalization of Par-1 upon PFC
219 ablation should enable microtubule growth in that region. Growth of microtubules from the posterior
220 towards the cytoplasm could explain the loss of *oskar* due to directed transport away from the cortex.
221 Indeed, in some oocytes we observed a local signal increase of the microtubule reporter Jupiter::GFP
222 where *oskar* signal decreased (Fig. 5D and Video 7). However, growth initiated considerably later than
223 *oskar* delocalization, so that in some oocytes we did not observe any growth within the time of
224 observation (Fig. 5E). Thus, this result shows that the maintenance of Par polarity by PFCs is functionally
225 important for robust microtubule cytoskeleton polarization. However, loss of *oskar* upon PFC ablation is
226 likely not caused by microtubule reorganization but rather from loss of cortical anchoring.

227 **aPKC kinetics after PFC ablation does not explain Par-1 removal from the posterior**

228 According to the current model of Par network polarization in the *Drosophila* oocyte, Par-1 is excluded
229 from the anterolateral membrane through phosphorylation by the kinase aPKC, which is recruited to the
230 membrane through interaction with Bazooka (Doerflinger et al., 2010). Conceivably, accumulation of
231 Bazooka at the posterior after PFC ablation may recruit aPKC, eventually leading to Par-1 delocalization
232 at the posterior. To obtain insight into the sequence of events, we performed live imaging of egg chambers
233 from flies that endogenously express aPKC::GFP (Fig. 6A and Video 8) (Chen et al., 2018) and
234 Bazooka::mCherry in the germline. Since both follicle cells and germline express aPKC, the initial
235 posterior exclusion of aPKC in the oocyte is masked by the apical signal in follicle cells. However, once

236 PFCs are ablated their aPKC::GFP signal disappears and any fluorescence detected can be associated to
237 aPKC in the oocyte (Fig. 6B, bottom row). Therefore, our assay allows us to unambiguously detect
238 possible accumulation of aPKC following ablation of PFCs. Although the signal of endogenously driven
239 protein expression is significantly lower when compared to using GAL4/UASp expression system, we
240 were able to observe accumulation of aPKC in most of the oocytes (Fig. 6B, arrowheads). An intensity
241 analysis of aPKC::GFP showed significant accumulation at stage 9. More importantly, aPKC localization
242 lagged upon perturbation and was always preceded by the accumulation of Bazooka (Fig. 6C–D).
243 Interestingly, we did not detect any significant increase in aPKC at stage 10A (Fig. 6D), which could be
244 explained by the signal detection limit in our imaging. More assuringly, the loss of Par-1 was on average
245 faster than the kinetics of aPKC ectopic localization after perturbation (Fig. 6E), suggesting that Par-1 loss
246 occurred before aPKC localized. We conclude that aPKC accumulation is insufficient for Par-1
247 displacement, and the maintenance of Par-1 localization at the posterior requires the oocyte to be in
248 contact with PFCs.

249 **Discussion**

250 In *Drosophila*, the canonical events of oocyte polarization ultimately lead to the delivery of mRNAs to
251 specific regions of the oocyte, which causes a symmetry break of gene expression that defines head and
252 tail of the future embryo (St Johnston and Nüsslein-Volhard, 1992). The main posterior determinant is
253 *oskar* mRNA, which is delivered to the posterior by two distinct processes – directed transport and
254 cytoplasmic streaming (Lu et al., 2018). Delivery by kinesin-dependent directed transport occurs during
255 stages 7–9 of oogenesis. Because plus end–directed kinesin transport is stochastic and insensitive to Par-1,
256 the microtubule cytoskeleton must be polarized so that microtubule plus–ends preferentially accumulate at
257 the posterior. This is achieved through Par-1 dependent inhibition of microtubule nucleation at the
258 posterior (Doerflinger et al., 2010; Nashchekin et al., 2016; Parton et al., 2011). Our results show that cell
259 contact with PFCs inhibits Bazooka accumulation and retains Par-1 localization at the posterior of the
260 oocyte. Therefore, PFCs have the crucial role in maintaining polarization of the microtubule cytoskeleton
261 during stages when *oskar* mRNA is delivered to the posterior by microtubule-mediated directed
262 transport. However, we also demonstrate that *oskar* accumulation at the posterior depends on Par-1
263 presence, and loss of posterior *oskar* occurs prior to changes in microtubule nucleation. At stage 10B, the
264 mechanism of directed transport is substituted by cytoplasmic streaming, which delivers mRNA particles
265 in bulk to the posterior where *oskar* is anchored by myosin V (Lu et al., 2018). Interestingly, this is the
266 stage at which we observe loss of contact between the PFCs and the oocyte, as well as the loss of Par
267 polarity. However, since polarization of the microtubule network is not necessary for cytoplasmic
268 streaming, this does not compromise *oskar* localization during late oogenesis. Instead of maintaining tight
269 contact between PFCs and the oocyte, molecular components building the eggshell can now be deposited
270 into the intercellular space by the follicle cells to prepare for egg maturation (Cavaliere et al., 2008).

271 In our current understanding of Par protein interaction and Par domain formation (reviewed in Hoege and
272 Hyman, 2013), the affinity of the posterior Par-1 for binding sites at the plasma membrane is modulated
273 by phosphorylation activity of anterior Par complex member aPKC. Par-1 can phosphorylate anterior Par
274 complex member Bazooka, which modulates the affinity of the anterior Par complex to bind to the
275 membrane or binding sites thereon. Because Par proteins exhibit diffusive properties at the membrane
276 (Goehring et al., 2011a), they not only accumulate by recruitment from the cytoplasm, but also move
277 laterally on the membrane and form reciprocal domains, where they remain unphosphorylated and have
278 high binding affinity. The antagonistic effect between anterior and posterior Pars is likely occurring
279 everywhere in the cell but is strongest where these proteins are most concentrated – at the plasma
280 membrane. This model can recapitulate Par domain formation, but it requires a trigger or initial symmetry
281 break that allows the reaction-diffusion network to converge towards stable domain formation. In *C.*
282 *elegans* the symmetry break is likely linked to the position of the centrosome provided by the sperm
283 (Bienkowska and Cowan, 2012; Goldstein and Hird, 1996). A biochemical signal from the centrosome
284 was proposed to locally inhibit actomyosin contractility and cause a local asymmetry in cortical flow
285 (Munro et al., 2004). Since anterior Pars are embedded within the cortex, they are displaced from the
286 posterior by advection allowing Par-1 (and Par-2) to accumulate from the cytoplasm (Goehring et al.,
287 2011b; Munro et al., 2004). While the inhibitory signal (cascade) emerging from the centrosome is yet to
288 be fully resolved (see Gan & Montegi, 2021 for a review), it is important to recognize in this model that
289 signal transmission is achieved by a mechanical process that removes the anterior Par complex from what
290 becomes the posterior domain. We show in the present study that, in the *Drosophila* oocyte, Bazooka
291 exclusion – or inhibition of its accumulation – at the posterior involves the mechanical transduction of
292 posterior follicle cell contact. This contact could either change the membrane composition, binding sites
293 thereon, or the hydrodynamic events close by, leading to locally distinct physical and chemical
294 circumstances for anterior Par proteins not to concentrate.

295 Both accumulation of Bazooka and delocalization of Par-1 following ablation of PFCs are restricted to the
296 membrane that was in direct contact with ablated follicle cells. We conclude that the remaining PFCs
297 continue transducing the signal that excludes Bazooka and retains Par-1. This agrees with previously
298 reported work studying mosaic mutants in components of signaling pathways that are necessary for
299 differentiation of PFCs (Frydman and Spradling, 2001; Poulton and Deng, 2006; Xi et al., 2003). In sum,
300 these studies showed that *oskar* mRNA and Staufen protein correctly localize to the membrane facing WT
301 follicle cells, while their localization is lost at the membrane facing neighboring cells that did not adopt
302 posterior fate. This observation argues against the idea that the polarizing signal is a diffusible molecule
303 within the extracellular space.

304 What distinguishes the cell-cell contact to PFCs from that of lateral follicle cells? Recent screening found
305 that components of extracellular matrix (ECM) and ECM-associated proteins are upregulated in PFCs
306 (Wittes and Schüpbach, 2019). Growing body of evidence suggests that there is a crosstalk between cell-

307 ECM and cell-cell adhesion (reviewed in Mui et al., 2016). For example, integrins have been reported to
308 increase the strength of cadherin adhesions (Martinez-Rico et al., 2010). Therefore, it is possible that
309 PFCs-ECM interaction affects the adhesion between the PFCs and the oocyte. Alternatively, differential
310 expression of eggshell genes occurs in the different subtypes of follicle cells. The eggshell is composed of
311 five distinct layers, for which the molecular components are secreted by the follicle cells. The first layer is
312 the vitelline membrane, which starts to be deposited at stage 9, at the time when Bazooka is excluded from
313 the posterior (Cavaliere et al., 2008). There are four vitelline membrane genes, one of which, *VM32E*, is
314 expressed in the main body follicle cells but not in the PFCs (Gargiulo et al., 1991). At stage 10, VM32E
315 protein is found at the interface between main body follicle cells and the oocyte, but not at the posterior
316 (Andrenacci et al., 2001). Interestingly, the protein spreads to the posterior by stage 11, which is the time
317 when the connection between the PFCs and the oocyte is lost. Therefore, it is possible that VM32E is
318 involved in separating follicle cells from the oocyte. Alternatively, the loss of contact between the PFCs
319 and the oocyte could be the consequence of deposition of the second layer of eggshell, a vax layer, which
320 starts at late stage 10 (Cavaliere et al., 2008).

321 Whatever the mechanism of keeping the oocyte and PFCs in close contact is, it seems to be important to
322 maintain Bazooka exclusion. Interestingly, the first anterior-posterior polarization event - positioning of
323 the oocyte to the posterior of the germline cyst at stage 1– is facilitated by cadherin mediated adhesion
324 between follicle cells and the oocyte (Godt and Tepass, 1998; González-Reyes and St Johnston, 1998). In
325 addition, the Par network becomes transiently polarized around this stage, with Par-1 at the posterior, and
326 Bazooka at the anterior of the oocyte (Vaccari and Ephrussi, 2002). Based on this, it has been suggested
327 that follicle cells are also involved in this first polarization of the oocyte (Roth and Lynch, 2009).

328 A change in adhesion between PFCs and the oocyte has been proposed as a mechanism by which the
329 polarizing signal could be transferred from the PFCs to the oocyte at stage 7 (Poulton and Deng, 2007).
330 How could the adhesion between follicle cells and the oocyte translate into oocyte polarization? Signals
331 derived from cell-cell contact are regulators of polarization in many cells and contexts (reviewed in Ebnet
332 et al., 2018). The most obvious downstream target of adhesion between the PFCs and the oocyte is the
333 actin cytoskeleton. Cell adhesion modulates actin organization and dynamics (reviewed in Bachir et al.,
334 2017). On the other hand, intact actin cytoskeleton is required both for posterior enrichment of Par-1 and
335 exclusion of Bazooka (Doerflinger et al., 2006; Jouette et al., 2019). Recently, myosin activation at the
336 posterior of the oocyte has been identified as the first known signal of oocyte polarity following the signal
337 from PFCs. A continuous local dephosphorylation of myosin regulatory light chain (MRLC) is necessary
338 for Par-1 localization (Doerflinger et al., 2022) and if would be interesting to understand the connection
339 between PFC contact signaling and MRCL phosphorylation state. It has been proposed that activated
340 myosin increases tension at the oocyte posterior, which might be necessary for recruitment of Par-1.
341 cadherin has been reported to promote recruitment and activation of myosin in epithelia (Shewan et al.,
342 2005). Therefore, it is possible that adhesion between the oocyte and PFCs causes specific activation of

myosin at the posterior. Alternatively, the polarizing cue could be transferred from PFCs to the oocyte through a trafficking dependent process. Endocytosis is elevated at the posterior of the oocyte, and this has been linked to posterior localization of *oskar* (Tanaka and Nakamura, 2008; Vanzo et al., 2007). Additionally, Bazooka is not excluded from the posterior following either knockdown of Rab-5 or expression of a dominant negative form of Rab-5 in the oocyte. On the contrary, overexpression of the PIP5Kinase Skittles (SKTL), which produces phosphoinositide PI(4,5)P2, bypasses the need for Par-1 to have Bazooka excluded from the posterior. PI(4,5)P2 plays a role in the first steps of endocytosis, suggesting that SKTL overexpression rescues Bazooka exclusion in *par-1* mutants by increasing endocytosis (Jouette et al., 2019). The trafficking could work either through direct delivery of a polarizing signal or by a passive process, for example by remodeling the posterior membrane or through membrane flows (Gerganova et al., 2021). Thus, future work should focus on the biophysics and molecular key players governing plasma membrane dynamics specifically at the oocyte–PFC interface.

Main Figures

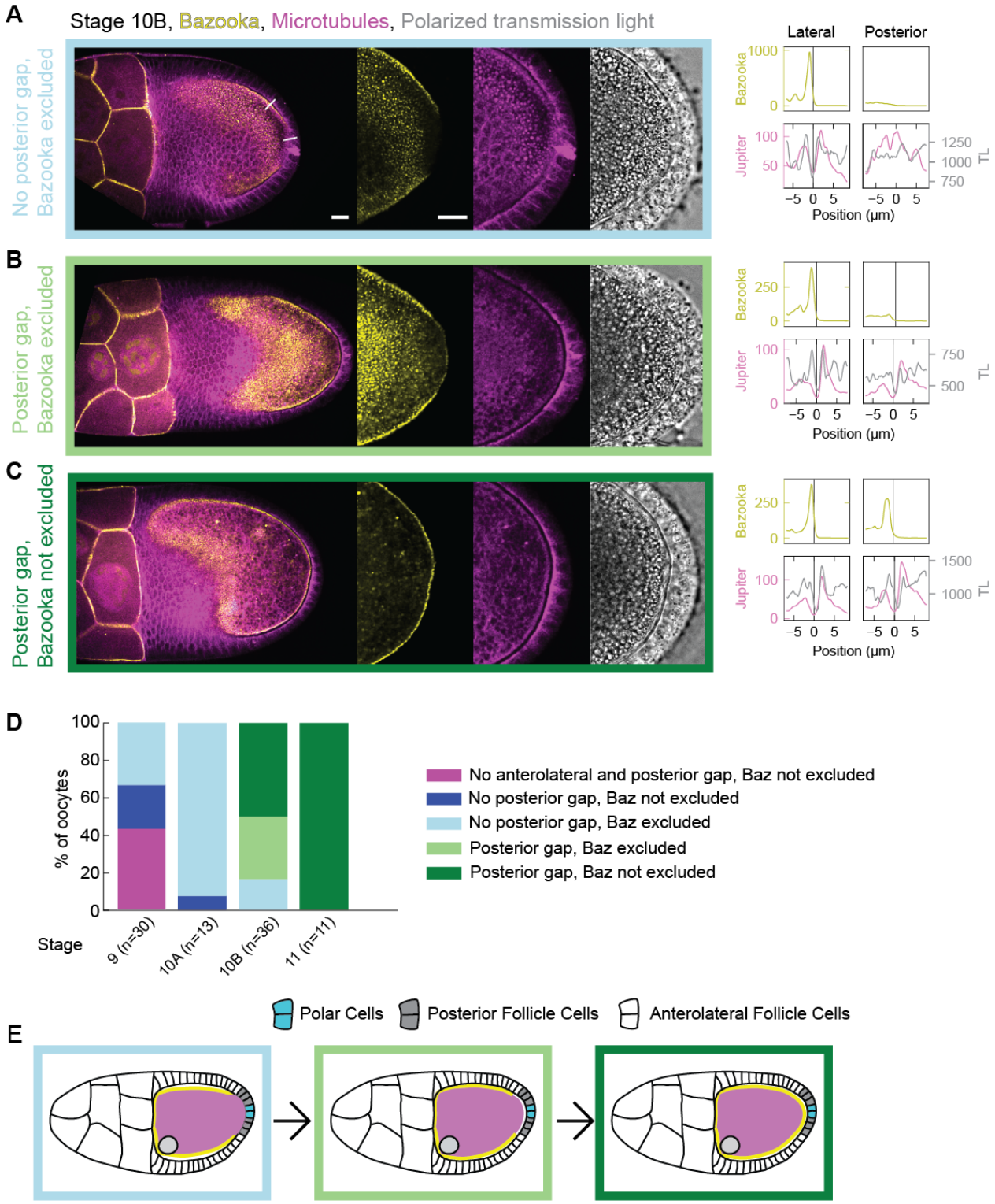

Figure 1. Bazooka accumulates at the posterior following the loss of contact between the oocyte and PFCs at stage 10B of oogenesis: (A–C) On the left are still images of stage 10B egg chambers expressing Bazooka::GFP (yellow) and the microtubule reporter Jupiter::mCherry (magenta) next to a transmission light micrograph (grey). The right graphs are intensity profiles of Bazooka::GFP (yellow), Jupiter::mCherry (magenta) and transmission light (grey) signal along a straight line crossing cell boundaries from the oocyte to either lateral or posterior follicle cells (see first image of the panel A). The

363 x-axis origin and vertical line represent the local minimum of the Jupiter::mCherry (magenta) signal,
364 which we interpret as extended intercellular space (gap) between the oocyte and the follicle cells.
365 Whenever this intercellular space is not clearly discernible, the position 0 µm represents the midpoint of
366 the line. **(A)** At the beginning of stage 10B, a gap is detected between the oocyte and the lateral follicle
367 cells but not the posterior follicle cells. Accumulation of Bazooka at the oocyte membrane correlates with
368 existence of the gap. **(B)** Later in stage 10B, a gap is formed at the posterior, but Bazooka does not yet
369 accumulate at the respective oocyte membrane. **(C)** Eventually, Bazooka accumulates to the posterior after
370 the formation of the gap. The scale bars represent 20 µm for panels A–C. **(D)** Distribution of egg
371 chambers showing one of the four possible phenotypes at stages 9, 10A, 10B and 11. Stage 9 is distinct
372 from later stages in that a fraction of egg chambers shows no (anterolateral) gap at all. The colors in the
373 plot correspond to the color of the frame surrounding the images in panels A–C. *n* is the number of egg
374 chambers quantified. **(E)** Scheme showing the timeline of events during stage 10B. Loss of contact
375 between the oocyte and PFCs precedes accumulation of Bazooka to the posterior.

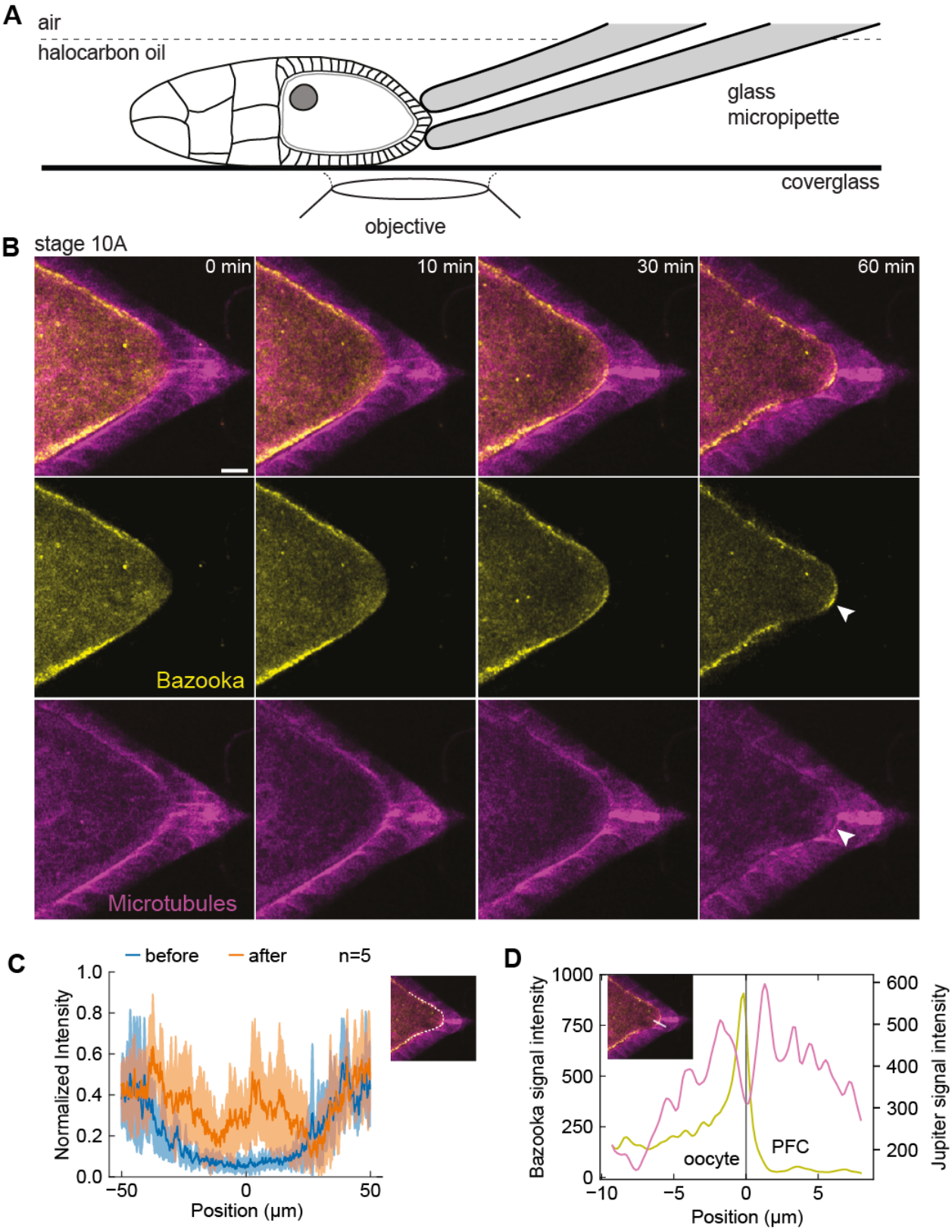

376

377 **Figure 2. Mechanical detachment of PFCs from the oocyte causes posterior accumulation of**
378 **Bazooka: (A)** Schematic showing experimental assay to mechanically detach PFCs from the oocyte. A
379 holding micropipette is used to aspirate and pull on the PFCs. **(B)** Time-lapse images of an egg chamber
380 expressing Bazooka::GFP (yellow) and the microtubule reporter Jupiter::mCherry (magenta) following

detachment of PFCs from the oocyte. Top: merged channels, middle: Bazooka::GFP, bottom: Jupiter::mCherry. Formation of the intercellular space and accumulation of Bazooka are detected at the posterior (arrowheads). Scale bar, 20 µm **(C)** The average intensity profile of Bazooka::GFP signal at the posterior of the oocyte, measured along the oocyte cortex as represented by the white line in the inset image. The blue curve is the intensity measured before the PFCs were pulled, the orange curve is the intensity after 60 min of continuous pulling. The shaded region designates the standard deviation. The x-axis origin represents the position of the polar cells. *n* is the number of experiments. **(D)** Intensity profile of Bazooka::GFP (yellow) and Jupiter::mCherry (magenta) along the line crossing cell boundaries from the oocyte to posterior follicle cells, as shown in the inset. The x-axis origin and vertical line represent the local minimum of the Jupiter::mCherry signal, which we interpret as intercellular space between the oocyte and the follicle cells.

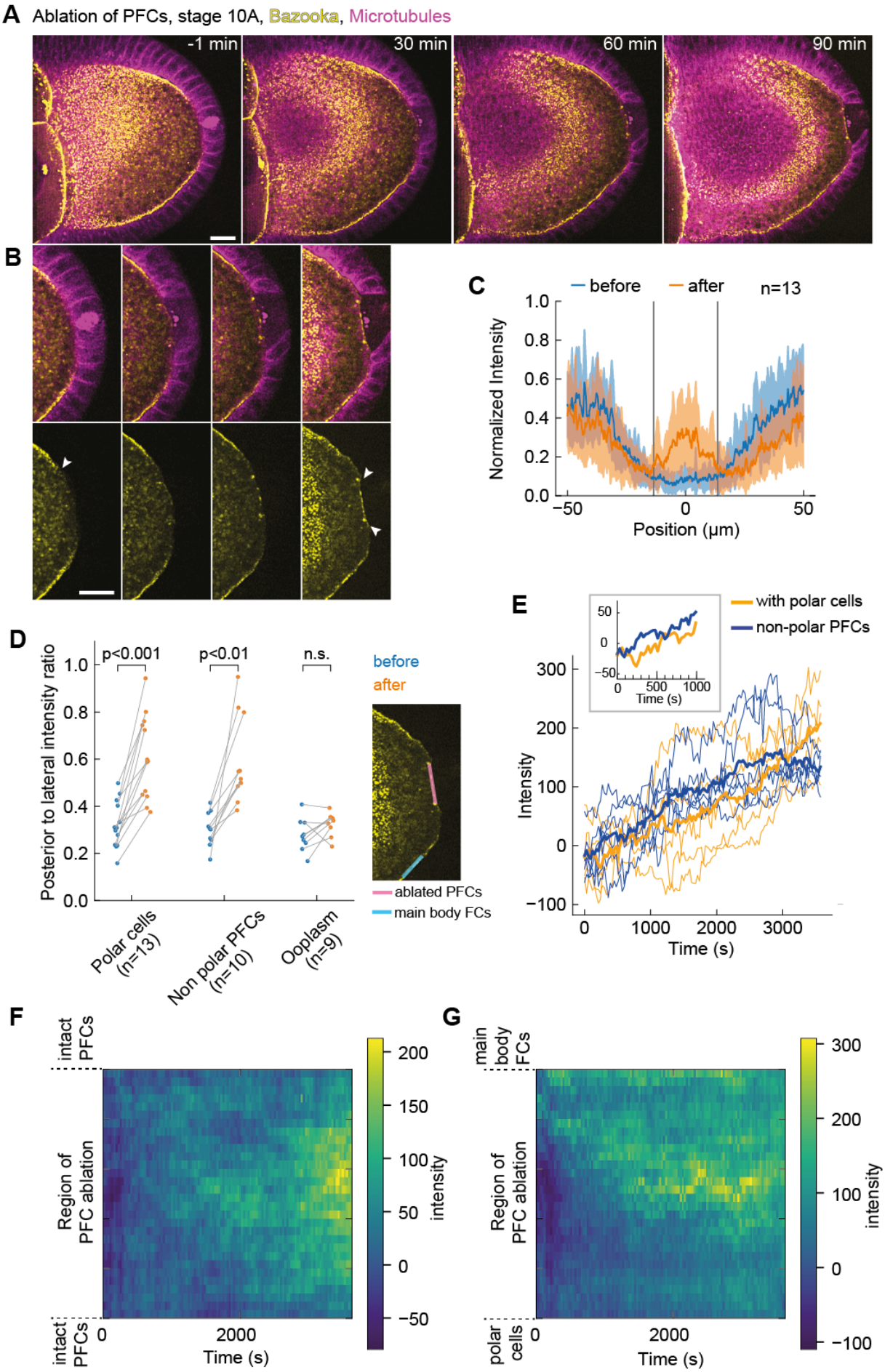
A
Ablation of PFCs, stage 10A, Bazooka, Microtubules
-1 min
30 min
60 min
90 min
B
C
before
after
n=13
Normalized Intensity
Position (μm)
D
p<0.001
p<0.01
n.s.
Posterior to lateral intensity ratio
Polar cells (n=13)
Non polar PFCs (n=10)
Ooplasm (n=9)
before
after
ablated PFCs
main body FCs
E
with polar cells
non-polar PFCs
Intensity
Time (s)
F
intact PFCs
Region of PFC ablation
intensity
Time (s)
G
main body FCs
Region of PFC ablation
polar cells
intensity
Time (s)

393 **Figure 3. Bazooka localizes to the posterior following ablation of PFCs: (A)** Two-color time-lapse
394 images of an egg chamber expressing Bazooka::GFP in the germline (yellow) and the microtubule reporter
395 Jupiter::mCherry (magenta) before (-1 min) and after ablation of PFCs. Scale bar, 20 µm. **(B)** Zoom-in of
396 the posterior end of the egg chamber shown in panel A. Top: merged channels, bottom: Bazooka::GFP.
397 Before ablation, Bazooka is excluded from the posterior, a region highlighted by the arrowheads in the
398 first image of the bottom panel. After 90 min, accumulation of Bazooka is visible at the oocyte membrane
399 facing the ablated cells (arrowheads in the last image). Scale bar, 20 µm. **(C)** Average intensity profile of
400 Bazooka::GFP signal at the posterior of the oocyte before (blue) and after (orange) ablation. The shaded
401 region designates the standard deviation. The x-axis origin represents the position of the ablated region.
402 Vertical lines denote the average width of the ablated region. Note that the increase of the signal is visible
403 only inside the ablated region. **(D)** Ratio between average Bazooka::GFP intensities along the oocyte
404 membrane facing ablated PFCs and lateral main body follicle cells, as depicted in the inset image, before
405 (blue) and after (orange) ablation for three types of ablation. PFCs: ablation of PFCs, including ablation of
406 polar cells (as in panel A). Non-polar PFCs: ablation of PFCs that do not include polar cells (see Suppl.
407 Fig. 2A). Ooplasm: ablation inside the ooplasm (see Suppl. Fig 2D). A ratio equal to 1 means complete
408 loss of Bazooka exclusion. Wilcoxon signed rank test was performed to assess significance (n.s.=not
409 significant). **(E)** Intensity of Bazooka::GFP signal at the oocyte membrane facing the ablated follicle cells
410 as a function of time, grouped in experiments where polar cells were ablated (orange, n=5) or left intact
411 (blue, n=5). The thick lines represent the average of each group, thin colored lines are individual oocytes.
412 Intensity of the ooplasm was subtracted from the Bazooka::GFP intensity, so that zero intensity (on
413 average) means exclusion of Bazooka. Inset: Average curves in the first 15 min. **(F)** Time series of
414 Bazooka::GFP intensity along the oocyte membrane facing ablated PFCs (y-axis) after PFC ablation,
415 represented as heat map. The ablated follicle cells included the polar cells, and the ablated region is
416 flanked by still intact PFCs. **(G)** As in panel F, but for ablations that excluded polar cells, so that the
417 ablated region was flanked by intact polar cells on one side (bottom of y-axis) and main body follicle cells
418 on the other side (top of y-axis). Note the signal inflow from the top of the graph. For all panels t = 0 is the
419 first frame after ablation, *n* is the number of experiments.

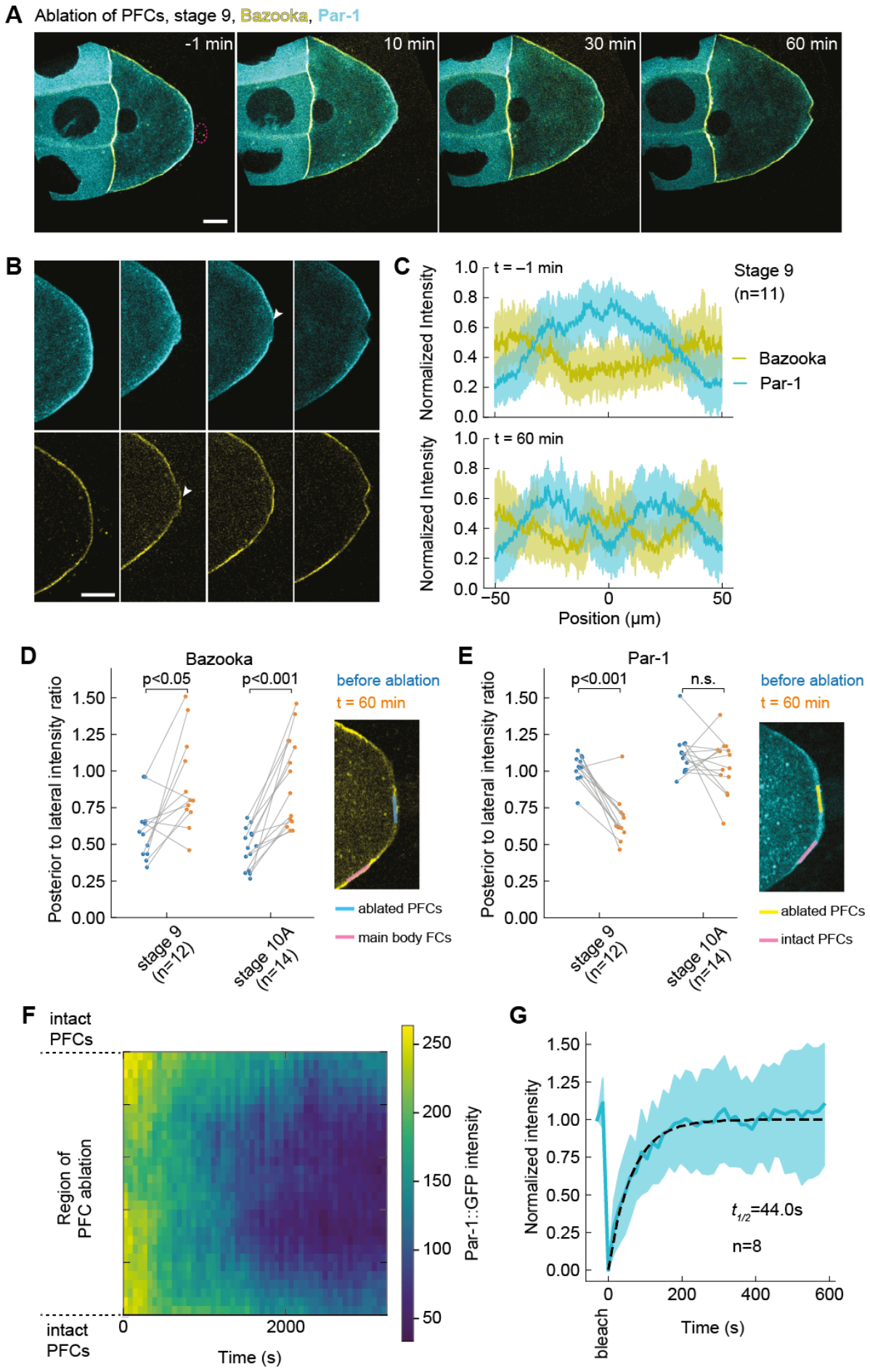
A
Ablation of PFCs, stage 9, Bazooka, Par-1
-1 min
10 min
30 min
60 min
B
C
t = –1 min
t = 60 min
Stage 9
(n=11)
Bazooka
Par-1
Normalized Intensity
Position (μm)
D
Bazooka
p<0.05
p<0.001
Posterior to lateral intensity ratio
stage 9 (n=12)
stage 10A (n=14)
before ablation
t = 60 min
ablated PFCs
main body FCs
E
Par-1
p<0.001
n.s.
intact PFCs
F
intact PFCs
Region of PFC ablation
Time (s)
Par-1::GFP intensity
G
Normalized intensity
$t_{1/2}$=44.0s
n=8
bleach
Time (s)

421 **Figure 4. Par-1 delocalizes slowly from the posterior despite fast turnover: (A)** Two-color time-lapse
422 images of an egg chamber at stage 9 expressing Par1::GFP (cyan) and Bazooka::mCherry (yellow) in the
423 germline, before (-1 min) and after ablation of PFCs (red dashed circle). Scale bar, 20 µm **(B)** Zoom into
424 the posterior of the egg chamber shown in panel A. Top: Par1::GFP, bottom: Bazooka::mCherry.
425 Following ablation, Bazooka accumulates to the posterior, while Par-1 is still present but slowly
426 delocalizing (arrowheads). Scale bar, 20 µm. **(C)** Average intensity profile of Par-1::GFP (cyan) and
427 Bazooka::mCherry (yellow) signal at the posterior of stage 9 oocytes before (top graph) and one hour after
428 ablation of PFCs (bottom graph). The shaded region designates the standard deviation. The x-axis origin
429 represents the position of the polar cells (top) or center of ablation spot (bottom). **(D)** Ratio between
430 Bazooka::mCherry intensities at the posterior and lateral membrane of the oocyte (facing main body
431 follicle cells), as depicted in the inset image, before (blue) and one hour after (orange) ablation. The ratio
432 0 signifies complete posterior exclusion, 1 and beyond denote localization. There is a significant increase
433 in the ratio for both stages 9 and 10A, showing accumulation of Bazooka to the posterior. **(E)** Ratio
434 between Par-1::GFP intensities at the membrane of the oocyte facing posterior ablated PFCs and intact
435 PFCs sightly lateral, as depicted in the inset image, before (blue) and one hour after (orange) ablation.
436 There is no significant reduction of the ratio in stage 10A which would indicate delocalization of Par-1.
437 Wilcoxon signed rank test was performed to assess significance (n.s. = not significant). **(F)** Time series of
438 Par-1::GFP intensity along the oocyte membrane facing ablated PFCs (y-axis) after PFC ablation,
439 represented as heat map. **(G)** Normalized signal recovery after fluorescence photobleaching for Par1::GFP
440 signal at the oocyte membrane. Thick blue line is mean, the shaded region designates the standard
441 deviation, the dashed line is the fitted curve obtained by fitting a single exponential function. For all
442 panels, *n* is the number of experiments.

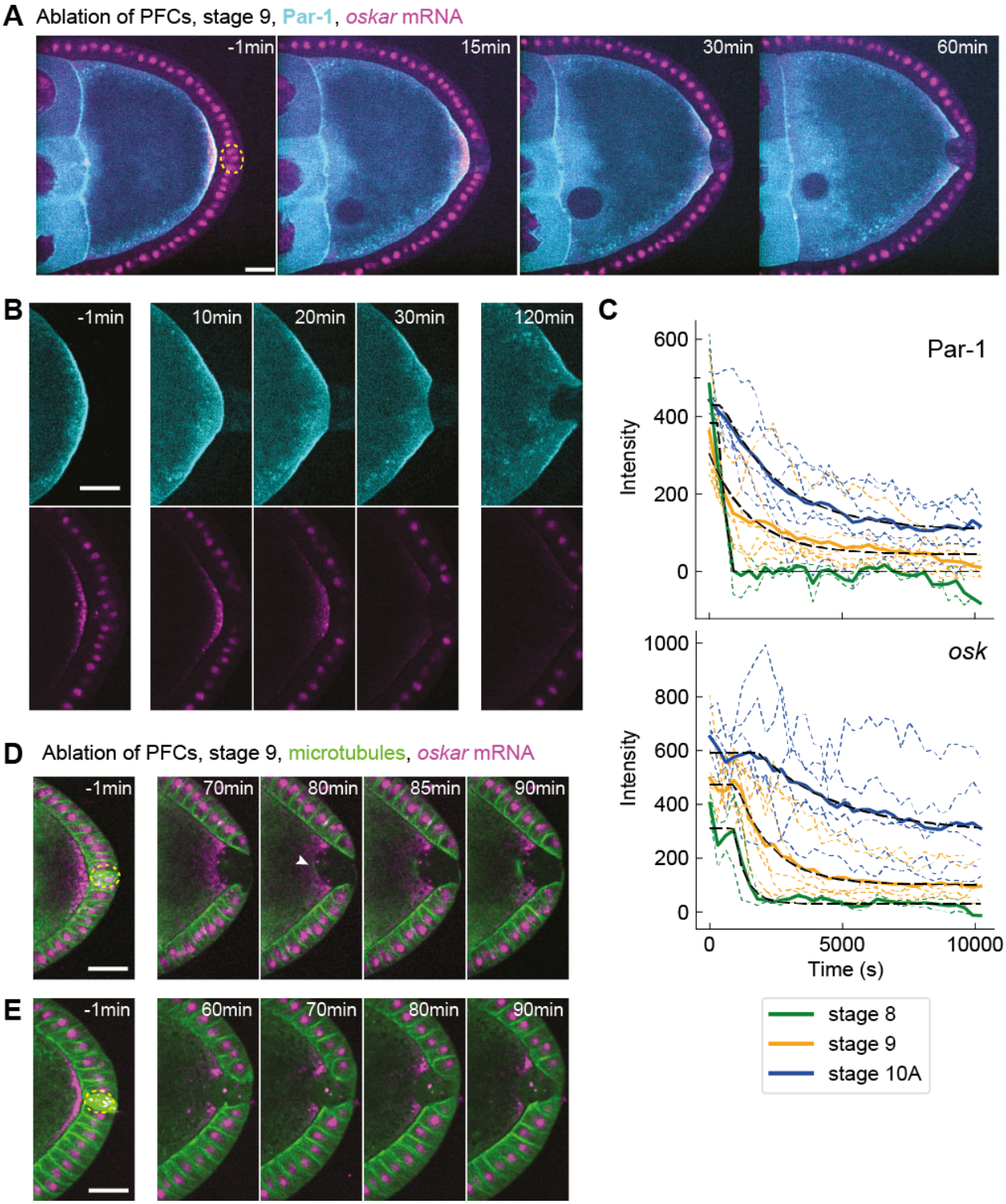

Figure 5. Posterior *oskar* mRNA is lost shortly after Par-1, and microtubules polymerize with long delay: (A) Two-color time-lapse images of an egg chamber expressing Par1::GFP in the germline (cyan) and *oskMS2*-mCherry (magenta) before (-1 min) and after ablation of PFCs (yellow dashed circle). Scale bar, 20 µm **(B)** Zoom-in of the posterior of the egg chamber shown in panel A. Top: Par-1::GFP, bottom: *oskMS2*-MCP::mCherry. Both Par-1 and *osk* delocalize from the cortex facing ablated PFCs. Scale bar, 20 µm. **(C)** Intensity of Par-1 (top) and *osk* mRNA (bottom) at the posterior of the oocyte facing ablated PFCs, for stages 8 (n=2), 9 (n=7) and 10A (n=6). Thin dashed lines are individual experiments, the solid

451 lines are the averages for each stage, and the black dashed line represents a fit to a single exponential
452 decay with time delay (see Methods). While Par-1 signal loss is immediate, *osk* mRNA decreases with
453 increasing delay; the estimated 95% CI (min) are for stage 8: [13.3, 16.5], for stage 9: [15.5, 18.9], for
454 stage 10A: [24.4, 36.0]. **(D)** Two-color time-lapse images of an egg chamber expressing Jupiter::GFP
455 (green) and *oskMS2*-mCherry (magenta) before (-1 min) and after ablation of PFCs. This example shows
456 microtubule growth at the posterior 80–90 min following ablation. Scale bar, 20 µm. **(E)** As in panel D,
457 showing an example of an oocyte that did not yet exhibit microtubule growth 90 min after PFC ablation.
458 Scale bar, 20 µm.

459

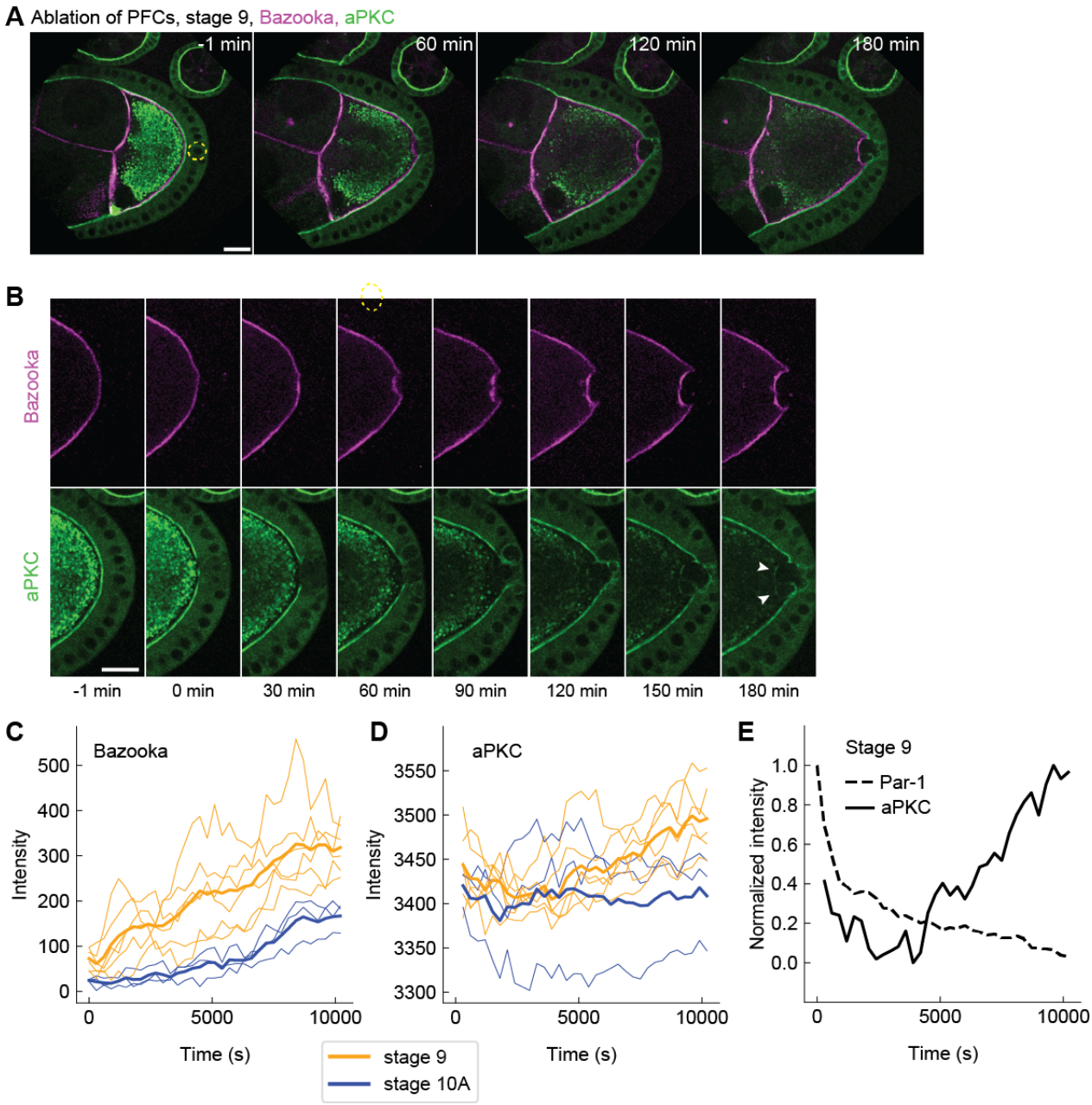

Figure 6. aPKC accumulates at the posterior after the changes in Bazooka and Par-1. (A) Two-color time-lapse images of an egg chamber at stage 9, expressing endogenous aPKC tagged with GFP (green) and Bazooka-mCherry in the germline (magenta) before (-1 min) and after ablation of PFCs (yellow dashed circle). Scale bar, 20 µm **(B)** Zoom-in of the posterior of the egg chamber shown in panel A. Top: Bazooka::mCherry, bottom: aPKC::GFP. While Bazooka accumulates within 60 minutes, aPKC is detectable only after 120–150 min (arrowheads). Scale bar, 20 µm. **(C)** Bazooka::mCherry intensity at the oocyte cortex facing the ablated PFCs, as a function of time for oocytes at stage 9 (orange, n=6) and 10A (blue, n=3). Thin lines are individual experiments, thick lines are stage averages. **(D)** As in panel C but for aPKC::GFP. Note the delayed increase in stage 9, and the lack of signal increase in stage 10A. **(E)** Normalized average intensities of Par1::GFP (dashed line) and aPKC::GFP (solid line) at stage 9 as a

471 function of time following the ablation of PFCs. Note the delay of aPKC signal increase. For all panels,
472 time zero marks the first frame after ablation.

473 # Materials and Methods

474 **Fly stocks and husbandry**

475 Fly husbandry was conducted in agreement with Portuguese National Regulations on Animal Welfare.

476 Fly lines used in this study:

Genotype	Origin / Gift	Reference
w; +; Jupiter::mCherry	Daniel St Johnston Lab	Lowe et al., 2014
w; +; Jupiter::GFP	Bloomington Drosophila Stock Center	#6836
w; UASp>GFP::Par-1(N1S)/CyO;+	Daniel St Johnston Lab	Huynh et al., 2001
w; UASp>Bazooka::mGFP/CyO;+	Daniel St Johnston Lab	Benton and St Johnston, 2003b
w; UASp>Bazooka::mCherry/CyO;+	Bloomington Drosophila Stock Center	#65844
w; GFP::aPKC; +	Eurico Morais-de-Sá Lab	Chen et al., 2018
w; mat-α4>Gal4; +	Bloomington Drosophila Stock Center	#7062
w; +; mat-α4>Gal4	Bloomington Drosophila Stock Center	#7063
w; +; osk>osk::MS2(10x)/TM3, Sb	Anne Ephrussi Lab	Zimyanin et al., 2008
w; hsp83>MCP::mCherry/CyO; +	Anne Ephrussi Lab	Gáspár et al., 2017; Weil et al., 2006

477

478 The UASp>GFP::Par-1(N1S) isoform rescues the *par-1* mutant (Doerflinger et al., 2006). The rescuing
479 activity of the UASp>Bazooka::mGFP transgene was demonstrated by Benton and St Johnston, 2003b. To
480 express UASp-transgenes, flies were crossed with mat-α4>Gal4 driver. The cross was kept at 25°C for 3-4
481 days, after which parents were removed from the vial, and the vial was transferred to 18°C for the
482 remaining time of the development. Viability and fertility tests were performed for all lines. Female
483 offspring of the desired genotype were collected in vials with 3-4 males and supplied with fresh yeast. The

484 flies were kept in vials at 18°C for 3-4 days before dissection. Detailed genotypes of flies used in the
485 experiments were:

486 w*, mata4>Gal4 / UASp>Bazooka::mGFP ; Jupiter:mCherry/Jupiter::mCherry (Fig. 1–3, Suppl. Fig.
487 1A–B and Suppl. Fig. 2)

488 w*; UASp>GFP::Par-1(N1S)/+ ; mata4>Gal4/Bazooka::mCherry (Suppl. Fig. 1C–E; Fig. 4, Suppl.
489 Fig. 3D–F)

490 w*; mata4>Gal4 / UASp>GFP::Par-1(N1S) ; Jupiter:mCherry/Jupiter::mCherry (Suppl. Fig. 3A–C)

491 w*; UASp>GFP::Par-1(N1S)/hsp83>MCP::mCherry; mata4>Gal4 /osk>osk::MS2(10x) (Fig. 5A–C)

492 w*; +/hsp83>MCP::mCherry; Jupiter::GFP/osk>osk::MS2(10x) (Fig,.5D–E)

493 w*; GFP::aPKC / UASp>Bazooka::mCherry; + / mata4>Gal4 (Fig. 6)

494 **Cleaning of coverslips and sample preparation**

495 22x22 mm No. 1.5 coverslip (Marienfeld) were placed in a ceramic rack, placed into a beaker with NaOH
496 (3M) and sonicated for 10 min. The rack was dipped-and-drained in a beaker with MilliQ water,
497 transferred to clean MilliQ water and sonicated for 10 min. Finally, the rack was transferred into a new
498 beaker with clean MilliQ water and sonicated for another 10 min. Coverslips were spin-dried and stored in
499 a clean rack and sealed container until final use.

500 For experiments shown in Fig. 1–3, ovaries were dissected in a drop of halocarbon oil (Voltalef 10S,
501 Arkema) placed on a clean coverslip, using tweezers to separate individual germaria. For experiments
502 shown in Fig. 4–6, ovaries were dissected in a drop of Schneider's medium supplemented with 10% FBS
503 and 200 µg/mL insulin. Dissected ovaries were incubated 2x30s in 20 µL of supplemented Schneider's
504 medium. Finally, ovaries were transferred to a drop of supplemented Schneider's medium on a clean
505 coverslip next to a drop of halocarbon oil and individual germaria were pulled into the oil. This latter
506 protocol improved the sample lifetime and allowed for longer time-lapse imaging.

507 **Microscopy**

508 Imaging was performed on a Nikon Eclipse Ti-E microscope equipped with a Yokogawa CSU-W
509 Spinning Disk confocal scanner and a piezoelectric stage (737.2SL, Physik Instrumente), using 40x water
510 immersion objective and 488 nm and 561 nm laser lines for excitation of GFP and mCherry, respectively.
511 Images were acquired at 73 focal planes with 0.5 µm z-spacing. x-y pixel size was 162 nm. An Andor
512 iXon3 888 EMCCD camera was used for time-lapse acquisitions, while an Andor Zyla 4.2 sCMOS
513 camera, which offers 2x wider field of view, was used for snapshot images of whole egg chambers for
514 analyses as shown in Fig. 1 and Suppl. Fig. 1. During time-lapse microscopy, images were acquired every
515 30 s (in experiments show in Fig. 2–3, Suppl Fig. 2, and Suppl. Fig. 3A–C) or every 60 s (in experiments

516 show in Fig. 4 and Suppl. Fig. 3D–F) for 60–90 minutes. To assess Par protein dynamics at longer
517 timescales (Fig. 5 and Fig. 6), images were acquired every 5 min for at least 150 minutes.

518 **Laser ablation**

519 The laser ablation system used in this study was described elsewhere (De-Carvalho et al., 2022). Follicle
520 cells were ablated using circular ablation (60 px diameter, 5 px step size). Ablation was performed several
521 times while moving manually in z direction to UV expose the entire depth of the cells. In samples which
522 were not dissected in Schneider's medium, ablation was performed 25 times using 50% laser power.
523 When sample was dissected in Schneider's medium laser ablation became more effective, presumably
524 because the egg chambers are surrounded by a thin layer of aqueous solution. Therefore, ablation in these
525 samples was performed 5 times using 20% laser power. To control for unspecific effects of laser ablation,
526 the ooplasm was ablated using identical power settings.

527 **Fluorescence recovery after photobleaching (FRAP)**

528 Par1::GFP at the oocyte membrane was bleached along ~100 px long line using the laser used for the
529 ablation (2% laser power, 1 px step size). Bleaching was performed in 10 z-planes with 0.5 µm spacing
530 between planes. Images were acquired every 15 s for 15 min. At least two images before photobleaching
531 were acquired.

532 **Image processing**

533 Image deconvolution was done in Huygens (Scientific Volume Imaging) using a theoretical point spread
534 function (PSF), 40 iterations, a signal-to-noise ratio of 8 and automatic brick layout. The background was
535 estimated by measuring the signal in areas where there was no egg chamber. Deconvolution was done
536 separately for each channel. Images shown in the figures were made by calculating the sum of 6 z-slices in
537 Fiji/ImageJ (National Institutes of Health; (Schindelin et al., 2012). Final figures were assembled in
538 Illustrator (Adobe).

539 **Image analysis**

540 All measurements were performed in Fiji/ImageJ on a sum of 6 z-slices. All measurements were
541 performed on raw images, except for the intensity profiles shown in Fig. 1A-C and Fig. 2D, which were
542 done on deconvolved images. The profiles were measured by drawing a 10 px wide line from the oocyte
543 to the follicle cells and measuring the mean intensity across the line in all three channels (Bazooka::GFP,
544 Jupiter::mCherry and polarized transmission light).

545 Profiles of signal intensities at the posterior membrane of the oocytes were calculated by drawing a 10 px
546 wide segmented line across the oocyte posterior cortex. Values of intensities for each frame were

normalized using min-max normalization. The zero position on the x-axis represents the reference point, i.e. the polar cells or the ablation spot.

To calculate the posterior to lateral intensity ratio, a 10 px wide and ~50 µm long line was drawn at the posterior and lateral membrane cortex of the oocyte. Mean intensity across this line was calculated and the mean value of the background signal was subtracted from this value. The background signal was measured by drawing a 10 px wide and ~50 µm long line in an area of the image where there was no egg chamber.

To measure the change in intensity over time, a 10 px wide segmented line was drawn, covering only the membrane that was previously in contact with ablated follicle cells. The line was manually moved if necessary due to x-y drift of the sample. Mean value of intensity across this line was measured in all time frames. Background signal was measured in the ooplasm next to the posterior membrane of the oocyte, using a 10 px wide and ~50 µm long line. Intensity shown in graphs was calculated by subtracting the mean value of the background signal from the mean intensity at the membrane. To produce the heatmaps, the profile of intensity across the line was obtained, and mean background signal was subtracted. Since the length of the ablation region was different in different experiments, the values of pixel intensities were binned into 30 bins. The final heatmaps show the intensity in 30 bins averaged over several experiments.

Mean fluorescence intensity of the photobleached region was measured by drawing a 10 px wide line over the region. To correct for photobleaching, the mean intensity of reference signal was measured inside the ooplasm. The background signal, measured outside of the egg chamber, was subtracted from the signal measured in both bleached and reference region. Normalized intensity was calculated as:

$$I = \frac{I_{ROI}}{I_{ROI,0}} \cdot \frac{I_{REF,0}}{I_{REF}}$$

Where I_{ROI} and I_{REF} are background subtracted intensity at the bleached region and reference region, respectively. $I_{ROI,0}$ and $I_{REF,0}$ are intensities before bleaching.

The normalized intensity was fitted to single exponential equations of the form:

$$I = 1 - e^{-kt}$$

Finally, the half-time of recovery was calculated as: $t_{1/2} = \frac{ln2}{k}$

Signal decays in Fig. 5 were fitted to a single exponential function with time delay τ as fitting parameter:

$$I = I_b + \begin{cases} I_0 & t < \tau \\ I_0\, e^{-\lambda t} & t \geq \tau \end{cases}$$

where I_b is the baseline intensity and I_0 is the signal amplitude decaying at rate λ.

Statistical analysis, curve fitting and plotting were done using Python. Information on sample size, statistical tests and p-values are shown in figures or mentioned in figure captions.

Acknowledgements

We thank members of the Telley lab for fruitful discussions. We acknowledge I. Gáspár and A. Ephrussi for suggestions on sample preparation. We thank the staff of the Fly Facility, the Advanced Imaging Facility (AIF) and the Technical Support Service at the Instituto Gulbenkian de Ciência (IGC). We thank Anne Ephrussi (EMBL Heidelberg), Daniel St. Johnston (The Gurdon Institute) and Eurico Morais-de-Sá (I3S Porto) for fly line donations, and The Bloomington Drosophila Stock Center for their services.

Funding

We acknowledge financial support from: Human Frontiers Science Program (HFSP) awarded to I.A.T. and supporting A.M. and J.C. (RGY0083/2016); the Fundação para Ciência e a Tecnologia (FCT) supporting I.A.T. (Investigador FCT IF/00082/2013) and A.M. (2020.04666.BD); Fundação Calouste Gulbenkian (FCG) and LISBOA-01-0145-FEDER-007654 supporting IGC's core operation; LISBOA-01-7460145-FEDER-022170 (Congento) supporting the Fly Facility; PPBI-POCI-01-0145-FEDER-022122 supporting the AIF, all co-financed by FCT (Portugal) and Lisboa Regional Operational Program (Lisboa2020) under the PORTUGAL2020 Partnership Agreement (European Regional Development Fund).

Author contributions

A.M. J.C., I.A.T. conceived the study; A.M. and J.C. established and validated the fly lines; A.M. designed and carried out all the experiments; A.M. and I.A.T. analyzed the data; I.A.T. designed and assembled the microscopy, micromanipulation, and laser ablation platform; A.M. wrote the draft manuscript guided by I.A.T.; all authors edited the final manuscript; I.A.T. supervised the project.

Competing interests

The authors have no competing financial or non-financial interests.

References

Andrenacci, D., Cernilogar, F.M., Taddei, C., Rotoli, D., Cavaliere, V., Graziani, F., and Gargiulo, G. (2001). Specific domains drive VM32E protein distribution and integration in Drosophila eggshell layers. J. Cell Sci. *114*, 2819–2829.

Bachir, A.I., Horwitz, A.R., Nelson, W.J., and Bianchini, J.M. (2017). Actin-based adhesion modules mediate cell interactions with the extracellular matrix and neighboring cells. Cold Spring Harb. Perspect. Biol. *9:a023234*, 1–19.

Benton, R., and St Johnston, D. (2003a). Drosophila PAR-1 and 14-3-3 Inhibit Bazooka / PAR-3 to Establish Complementary Cortical Domains in Polarized Cells. Cell *115*, 691–704.

Benton, R., and St Johnston, D. (2003b). A Conserved Oligomerization Domain in Drosophila

610 Bazooka/PAR-3 Is Important for Apical Localization and Epithelial Polarity. Curr. Biol. *13*, 1330–1334.

611 Bienkowska, D., and Cowan, C.R. (2012). Centrosomes can initiate a polarity axis from any position
612 within one-cell C. Elegans embryos. Curr. Biol. *22*, 583–589.

613 Cavaliere, V., Bernardi, F., Romani, P., Duchi, S., and Gargiulo, G. (2008). Building up the Drosophila
614 eggshell: First of all the eggshell genes must be transcribed. Dev. Dyn. *237*, 2061–2072.

615 Chen, J., Sayadian, A.C., Lowe, N., Lovegrove, H.E., and St Johnston, D. (2018). An alternative mode of
616 epithelial polarity in the Drosophila midgut. PLoS Biol. *16*, 1–24.

617 De-Carvalho, J., Tlili, S., Hufnagel, L., Saunders, T.E., and Telley, I.A. (2022). Aster repulsion drives
618 short-ranged ordering in the Drosophila syncytial blastoderm. Development *149*, 1–13.

619 Doerflinger, H., Benton, R., Torres, I.L., Zwart, M.F., and St Johnston, D. (2006). Drosophila Anterior-
620 Posterior Polarity Requires Actin-Dependent PAR-1 Recruitment to the Oocyte Posterior. Curr. Biol. *16*,
621 1090–1095.

622 Doerflinger, H., Vogt, N., Torres, I.L., Mirouse, V., Koch, I., Nüsslein-volhard, C., and St Johnston, D.
623 (2010). Bazooka is required for polarisation of the Drosophila anterior-posterior axis. Development *137*,
624 1765–1773.

625 Doerflinger, H., Zimyanin, V., and St Johnston, D. (2022). The Drosophila anterior-posterior axis is
626 polarized by asymmetric myosin activation. Curr. Biol. *32*, 374-385.e4.

627 Ebnet, K., Kummer, D., Steinbacher, T., Singh, A., Nakayama, M., and Matis, M. (2018). Regulation of
628 cell polarity by cell adhesion receptors. Semin. Cell Dev. Biol. *81*, 2–12.

629 Frydman, H.M., and Spradling, A.C. (2001). The receptor-like tyrosine phosphatase Lar is required for
630 epithelial planar polarity and for axis determination within Drosophila ovarian follicles. Development *128*,
631 3209–3220.

632 Gargiulo, G., Gigliotti, S., Malva, C., and Graziani, F. (1991). Cellular specificity of expression and
633 regulation of Drosophila vitelline membrane protein 32E gene in the follicular epithelium: identification
634 of cis-acting elements. Mech. Dev. *35*, 193–203.

635 Gáspár, I., Sysoev, V., Komissarov, A., and Ephrussi, A. (2017). An RNA-binding atypical tropomyosin
636 recruits kinesin-1 dynamically to oskar mRNPs. EMBO J. *36*, 319–333.

637 Gerganova, V., Lamas, I., Rutkowski, D.M., Vještica, A., Castro, D.G., Vincenzetti, V., Vavylonis, D.,
638 and Martin, S.G. (2021). Cell patterning by secretion-induced plasma membrane flows. Sci. Adv. *7*, 1–19.

639 Godt, D., and Tepass, U. (1998). Drosophila oocyte localization is mediated by differential cadherin-
640 based adhesion. Nature *395*, 387–391.

641 Goehring, N.W., Hoege, C., Grill, S.W., and Hyman, A.A. (2011a). PAR proteins diffuse freely across the
642 anterior–posterior boundary in polarized. J. Cell Biol. *193*, 583–594.

643 Goehring, N.W., Khuc Trong, P., Bois, J.S., Chowdhury, D., Nicola, E.M., Hyman, A.A., and Grill, S.W.
644 (2011b). Polarization of PAR Proteins by Advective Triggering of a Pattern-Forming System. Science
645 (80-.). *334*, 1137–1141.

646 Goldstein, B., and Hird (1996). Specification of the anteroposterior axis in Caenorhabditis elegans.
647 Development *122*, 1467–1474.

648 González-Reyes, A., and St Johnston, D. (1994). Role of Oocyte Position in Establishment of Anterior-
649 Posterior Polarity in Drosophila. Science (80-.). *266*, 639–642.

650 González-Reyes, A., and St Johnston, D. (1998). The Drosophila AP axis is polarised by the cadherin-
651 mediated positioning of the oocyte. Development *125*, 3635–3644.

652 González-Reyes, A., Elliot, H., and St Johnston, D. (1995). Polarization of both major body axes in

653 Drosophila by gurken-torpedo signalling. Nature *375*, 654–658.

654 Hoege, C., and Hyman, A.A. (2013). Principles of PAR polarity in Caenorhabditis elegans embryos. Nat.
655 Rev. Mol. Cell Biol. *14*, 315–322.

656 Huynh, J.-R., Shulman, J.M., Benton, R., and St Johnston, D. (2001). PAR-1 is required for the
657 maintenance of oocyte fate in Drosophila. Development *128*, 1201–1209.

658 Jouette, J., Guichet, A., and Claret, S.B. (2019). Dynein-mediated transport and membrane trafficking
659 control PAR3 polarised distribution. Elife *8:e402128*, 1–28.

660 Lang, C.F., and Munro, E. (2017). The PAR proteins : from molecular circuits to dynamic self-stabilizing
661 cell polarity. Development *144*, 3405–3416.

662 Lowe, N., Rees, J.S., Roote, J., Ryder, E., Armean, I.M., Johnson, G., Drummond, E., Spriggs, H.,
663 Drummond, J., Magbanua, J.P., et al. (2014). Analysis of the expression patterns, Subcellular localisations
664 and interaction partners of drosophila proteins using a pigp protein trap library. Development *141*, 3994–
665 4005.

666 Lu, W., Lakonishok, M., Serpinskaya, A.S., Kirchenbüechler, D., Ling, S.C., and Gelfand, V.I. (2018).
667 Ooplasmic flow cooperates with transport and anchorage in Drosophila oocyte posterior determination. J.
668 Cell Biol. *217*, 3497–3511.

669 Lu, W., Lakonishok, M., Liu, R., Billington, N., Rich, A., Glotzer, M., Sellers, J.R., and Gelfand, V.I.
670 (2020). Competition between kinesin-1 and myosin-V defines Drosophila posterior determination. Elife
671 *9:e54216*, 1–25.

672 Martinez-Rico, C., Pincet, F., Thiery, J.P., and Dufour, S. (2010). Integrins stimulate E-cadherin-mediated
673 intercellular adhesion by regulating Src-kinase activation and actomyosin contractility. J. Cell Sci. *123*,
674 712–722.

675 Motegi, F., and Seydoux, G. (2013). The PAR network: Redundancy and robustness in a symmetry-
676 breaking system. Philos. Trans. R. Soc. B Biol. Sci. *368*, 20130010.

677 Mui, K.L., Chen, C.S., and Assoian, R.K. (2016). The mechanical regulation of integrin-cadherin crosstalk
678 organizes cells, signaling and forces. J. Cell Sci. *129*, 1093–1100.

679 Munro, E., Nance, J., and Priess, J.R. (2004). Cortical flows powered by asymmetrical contraction
680 transport PAR proteins to establish and maintain anterior-posterior polarity in the early C. elegans embryo.
681 Dev. Cell *7*, 413–424.

682 Nashchekin, D., Ribeiro Fernandes, A., and St Johnston, D. (2016). Patronin / Shot Cortical Foci
683 Assemble the Noncentrosomal Microtubule Array that Specifies the Drosophila Anterior-Posterior Axis.
684 Dev. Cell *38*, 61–72.

685 Parton, R.M., Hamilton, R.S., Ball, G., Yang, L., Cullen, C.F., Lu, W., Ohkura, H., and Davis, I. (2011). A
686 PAR-1–dependent orientation gradient of dynamic microtubules directs posterior cargo transport in the
687 Drosophila oocyte. J. Cell Biol. *194*, 121–135.

688 Poulton, J.S., and Deng, W.-M. (2006). Dystroglycan down-regulation links EGF receptor signaling and
689 anterior-posterior polarity formation in the Drosophila oocyte. Proc. Natl. Acad. Sci. *103*, 12775–12780.

690 Poulton, J.S., and Deng, W.M. (2007). Cell-cell communication and axis specification in the Drosophila
691 oocyte. Dev. Biol. *311*, 1–10.

692 Riechmann, V., and Ephrussi, A. (2001). Axis formation during Drosophila oogenesis. Curr. Opin. Genet.
693 Dev. *11*, 374–383.

694 Roth, S., and Lynch, J.A. (2009). Symmetry Breaking During Drosophila Oogenesis. Cold Spring Harb.
695 Perspect. Biol. *1:a001891*, 1–22.

696 Roth, S., Neuman-Silberberg, F.S., Barcelo, G., and Schüpbach, T. (1995). cornichon and the EGF

Receptor Signaling Process Are Necessary for Both Anterior-Posterior and Dorsal-Ventral Pattern Formation in Drosophila. Cell *81*, 967–978.

Schindelin, J., Arganda-Carreras, I., Frise, E., Kaynig, V., Longair, M., Pietzsch, T., Preibisch, S., Rueden, C., Saalfeld, S., Schmid, B., et al. (2012). Fiji: An open-source platform for biological-image analysis. Nat. Methods *9*, 676–682.

Shewan, A.M., Maddugoda, M., Kraemer, A., Stehbens, S.J., Verma, S., Kovacs, E.M., and Yap, A.S. (2005). Myosin 2 Is a Key Rho Kinase Target Necessary for the Local Concentration of E-Cadherin at Cell–Cell Contacts. Mol. Biol. Cell *16*, 4531–4542.

Shulman, J.M., Benton, R., and St Johnston, D. (2000). The Drosophila Homolog of C . elegans PAR-1 Organizes the Oocyte Cytoskeleton and Directs oskar mRNA Localization to the Posterior Pole. Cell *101*, 377–388.

St Johnston, D., and Nüsslein-Volhard, C. (1992). The origin of pattern and polarity in the Drosophila embryo. Cell *68*, 201–219.

Tanaka, T., and Nakamura, A. (2008). The endocytic pathway acts downstream of Oskar in Drosophila germ plasm assembly. Development *135*, 1107–1117.

Tomancak, P., Piano, F., Riechmann, V., Gunsalus, K.C., Kemphues, K.J., and Ephrussi, A. (2000). A Drosophila melanogaster homologue of Caenorhabditis elegans par-1 acts at an early step in embryonic-axis formation. Nat. Cell Biol. *2*, 458–460.

Vaccari, T., and Ephrussi, A. (2002). The fusome and microtubules enrich Par-1 in the oocyte, where it effects polarization in conjunction with Par-3, BicD, Egl, and Dynein. Curr. Biol. *12*, 1524–1528.

Vanzo, N., Oprins, A., Xanthakis, D., Ephrussi, A., and Rabouille, C. (2007). Stimulation of Endocytosis and Actin Dynamics by Oskar Polarizes the Drosophila Oocyte. Dev. Cell *12*, 543–555.

Weil, T.T., Forrest, K.M., and Gavis, E.R. (2006). Localization of bicoid mRNA in Late Oocytes Is Maintained by Continual Active Transport. Dev. Cell *11*, 251–262.

Wittes, J., and Schüpbach, T. (2019). A gene expression screen in Drosophila melanogaster identifies novel JAK/STAT and EGFR targets during oogenesis. G3 Genes, Genomes, Genet. *9*, 47–60.

Xi, R., McGregor, J.R., and Harrison, D.A. (2003). A gradient of JAK pathway activity patterns the anterior-posterior axis of the follicular epithelium. Dev. Cell *4*, 167–177.

Zimyanin, V.L., Belaya, K., Pecreaux, J., Gilchrist, M.J., Clark, A., Davis, I., and St Johnston, D. (2008). In Vivo Imaging of oskar mRNA Transport Reveals the Mechanism of Posterior Localization. Cell *134*, 843–853.

Supplementary Figures

Suppl. Figure 1:

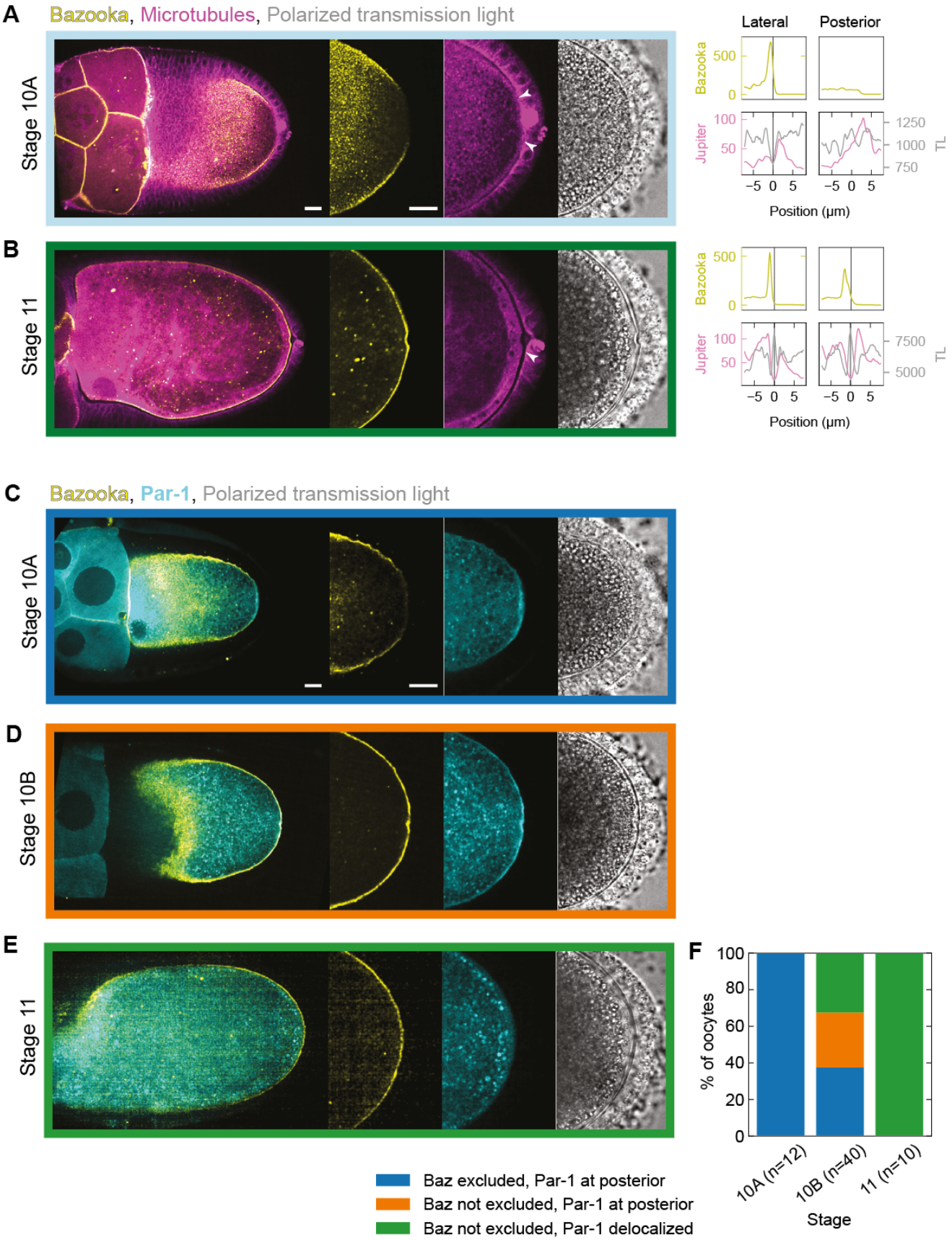

731 **Suppl. Figure 1: Localization of Bazooka and Par-1 during stages 10 and 11 of oogenesis:** On the left
732 are still images of stage 10A **(A)** and 11 **(B)** egg chambers expressing Bazooka::GFP (yellow) and the
733 microtubule reporter Jupiter::mCherry (magenta) next to a transmission light micrograph (grey). The right
734 graphs are intensity profiles of Bazooka::GFP (yellow), Jupiter::mCherry (magenta) and transmission light
735 (grey) signal along a straight line crossing cell boundaries from the oocyte to either lateral or posterior
736 follicle cells. The x-axis origin and the vertical line represent the local minimum of the Jupiter::mCherry
737 (magenta) signal, which we interpret as extended intercellular space (gap) between the oocyte and the
738 follicle cells. If the intercellular space is not clearly discernible, the position 0 µm represents the midpoint
739 of the line. **(A)** At stage 10A, the gap is visible between the oocyte and the lateral follicle cells, but not
740 between the oocyte and the posterior follicle cells. Accumulation of Bazooka correlates with the existence
741 of the gap. **(B)** At stage 11, both the gap and Bazooka accumulation are visible at the posterior. **(C–E)**
742 Stage 10A, 10B and 11 egg chambers expressing Bazooka::mCherry (yellow) and Par-1::GFP (cyan) in
743 the germline. At stage 10A, the mutual exclusion zone between Bazooka and Par-1 exists at the posterior.
744 During stage 10B Bazooka accumulates to the posterior before delocalization of Par-1. At stage 11, both
745 exclusion of Bazooka and accumulation of Par-1 at the posterior are lost. **(F)** Distribution of egg chambers
746 showing different posterior Par protein localization patterns. The colors in the plot correspond to the color
747 of the frame surrounding the images in panels C–E. Note that Par-1 delocalization never precedes
748 accumulation of Bazooka. Scale bars represent 20 µm, *n* is the number of egg chambers.

Suppl. Figure 2:

A Ablation of non polar PFCs, stage 10A, Bazooka, Microtubules

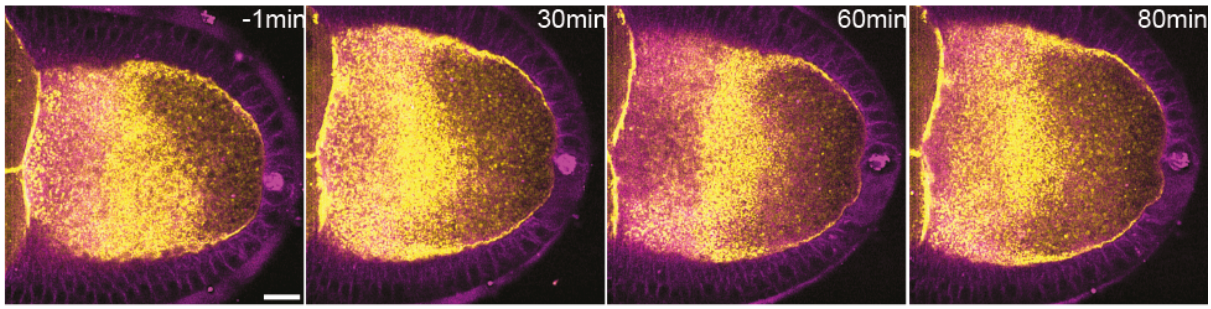

B

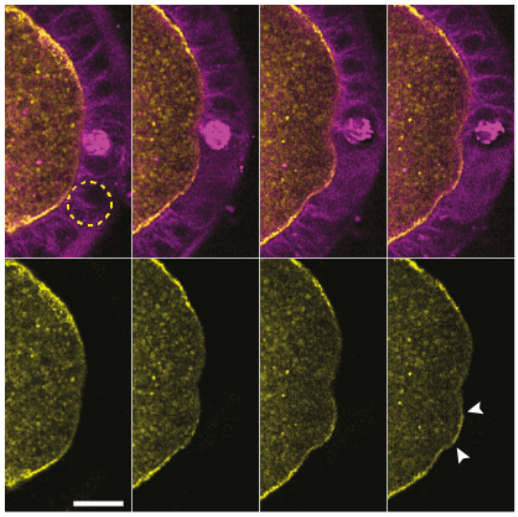

C

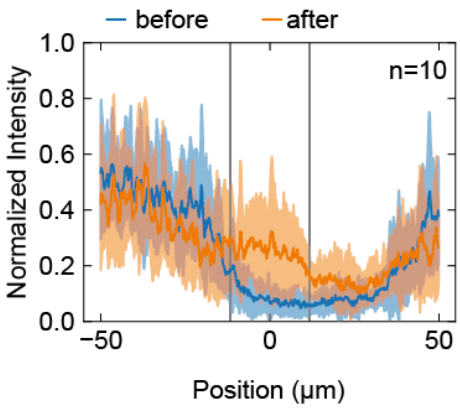

D Ablation of ooplasm, stage 10A, Bazooka, Microtubules

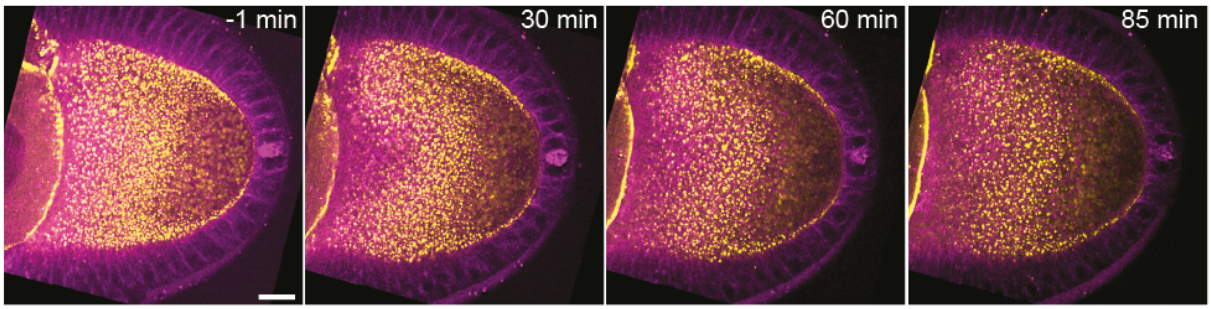

E

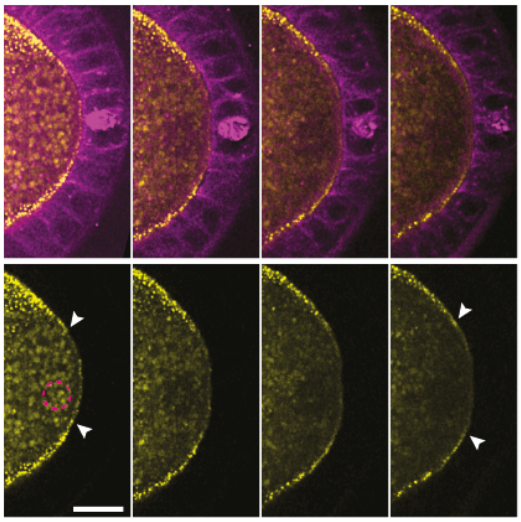

F

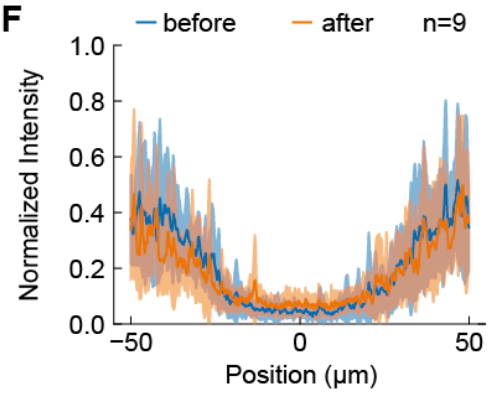

750 **Suppl. Figure 2: Bazooka localizes to the posterior following ablation of PFCs: (A)** Two-color time-
751 lapse images of an egg chamber expressing Bazooka::GFP in the germline (yellow) and the microtubule
752 marker Jupiter::mCherry (magenta) before (-1 min) and after ablation of PFCs. **(B)** Zoom-in of the
753 posterior of the egg chamber shown in panel A. Top: merged channels, bottom: Bazooka::GFP. Dashed
754 circle in the first image of the top panel represents the ablation spot. Note that polar cells (pair of cells
755 with high Jupiter signal) are not ablated. After 80 min, the accumulation of Bazooka::GFP is visible at the
756 oocyte membrane facing the ablated cells (arrowheads in last image). **(C)** Average intensity profile of
757 Bazooka::GFP signal at the posterior of the oocyte before (blue) and after (orange) ablation. The shaded
758 region represents the standard deviation. The x-axis origin represents the position of the ablated region.
759 Vertical lines denote the average width of the ablated region. Note that the signal increases markedly only
760 within the ablated region. **(D)** Two-color time-lapse images of an egg chamber expressing Bazooka::GFP
761 in the germline (yellow) and microtubule marker Jupiter::mCherry (magenta) before (-1 min) and after
762 ablation within the ooplasm. **(E)** Zoom-in of the posterior of the egg chamber shown in panel D. Top:
763 merged channels, bottom: Bazooka::GFP. Dashed circle in the first image of the bottom panel shows the
764 position of the ablation spot. Bazooka remains excluded from the posterior after ablation (arrowheads). **(F)**
765 Average intensity profile of Bazooka::GFP signal at the posterior of the oocyte before (blue) and after
766 (orange) ablation within the ooplasm. The shaded region designates the standard deviation. The x-axis
767 origin represents the position of polar cells. For all panels the scale bar represents 20 μm, and *n* is the
768 number of experiments.

Suppl. Figure 3:

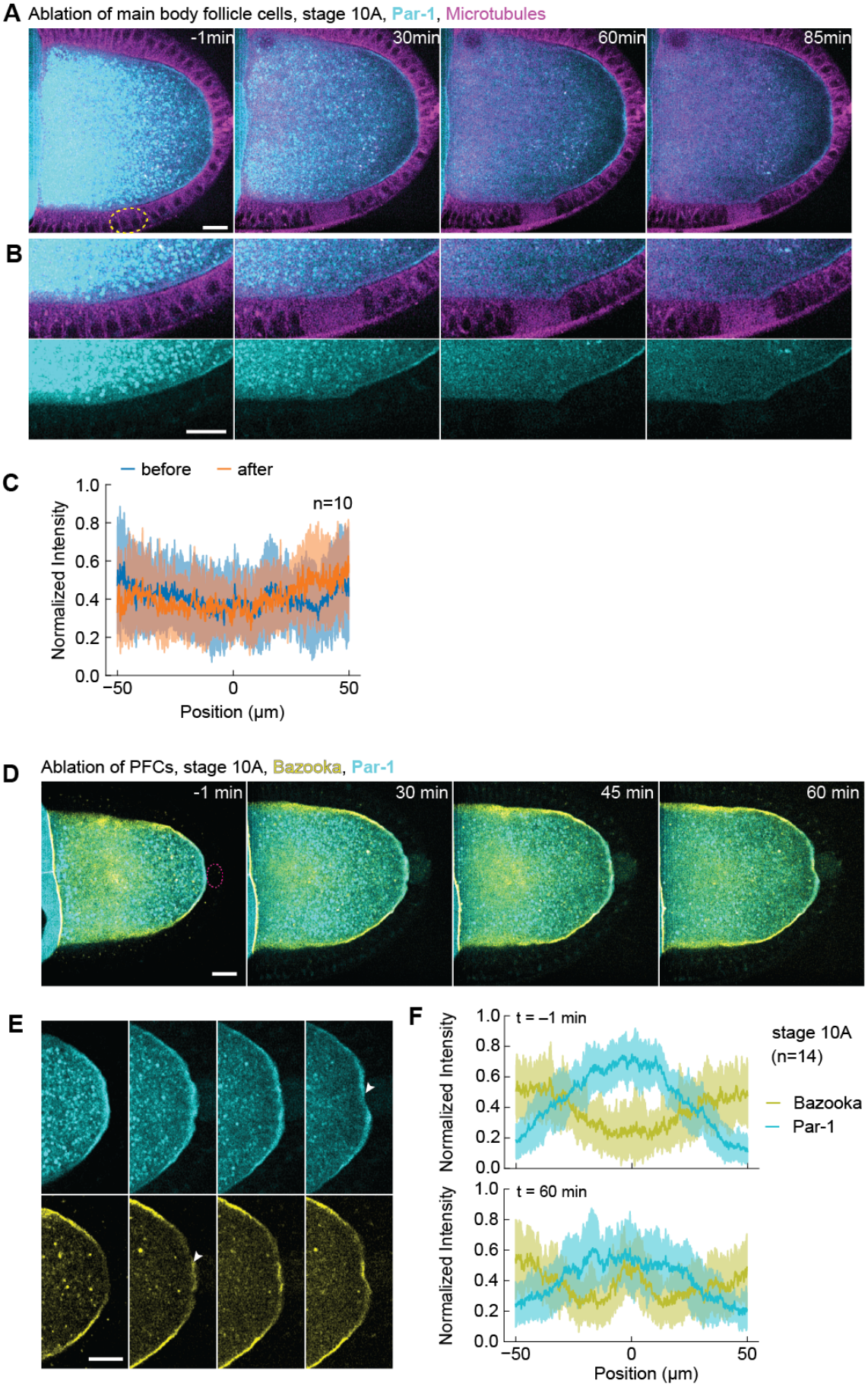

770 **Suppl. Figure 3. Par-1 loss from the posterior following PFC ablation is slower in stage 10A oocytes.**

771 **(A)** Two-colour time-lapse images of a control experiment on an egg chamber expressing Par-1::GFP in
772 the germline (cyan) and Jupiter::mCherry (magenta) before (-1 min) and after ablation of main body
773 follicle cells (yellow dashed circle). **(B)** Zoom-in of the lateral side of the egg chamber shown in panel A.
774 Top: merged channels, bottom: Par-1::GFP. No change in Par-1 localization is observed. **(C)** Average
775 intensity profile of Par-1::GFP signal around the ablated region before (blue) and after (orange) ablation of
776 the main body follicle cells. The shaded region designates the standard deviation. The x-axis origin
777 represents the center of the ablated region. **(D)** Two-color time-lapse images of an egg chamber at stage
778 10A expressing Par1::GFP (cyan) and Bazooka::mCherry (yellow) in the germline, before (-1 min) and
779 after ablation of PFCs (red dashed circle). Scale bar, 20 µm **(E)** Zoom into the posterior of the egg
780 chamber shown in panel A. Top: Par1::GFP, bottom: Bazooka::mCherry. Following ablation, Bazooka
781 accumulates to the posterior, while Par-1 marginally delocalizes (arrowheads). Scale bar, 20 µm. **(F)**
782 Average intensity profile of Par-1::GFP (cyan) and Bazooka::mCherry (yellow) signal at the posterior of
783 stage 10A oocytes before (top graph) and one hour after ablation of PFCs (bottom graph). The shaded
784 region designates the standard deviation. The x-axis origin represents the position of the polar cells (top)
785 or center of ablation spot (bottom). Note that Par-1 signal does not decrease much.

786

787 ## Supplementary Video Legends

788 **Video 1.** Sum of 6 z-slices from a time-lapse movie of stage 10A egg chamber expressing Bazooka::GFP
789 (yellow) and microtubule marker Jupiter::mCherry (magenta) following detachment of PFCs from the
790 oocyte. Left: polarized transmission light, right: florescence. Frame rate is 10 frames/s. In support of Fig.
791 2.

792 **Video 2.** Sum of 6 z-slices from a time-lapse movie of stage 10A egg chamber expressing Bazooka::GFP
793 (yellow) and microtubule marker Jupiter::mCherry (magenta). PFCs were ablated at time 0. Frame rate is
794 10 frames/s. In support of Fig. 3.

795 **Video 3.** Sum of 6 z-slices from a time-lapse movie of stage 10A egg chamber expressing Bazooka::GFP
796 (yellow) and microtubule marker Jupiter::mCherry (magenta). Ooplasm was ablated at time 0. Frame rate
797 is 10 frames/s. In support of Suppl. Fig. 2.

798 **Video 4.** Sum of 6 z-slices from a time-lapse movie of stage 9 egg chamber expressing Par1::GFP (cyan)
799 and Bazooka::mCherry (yellow). PFCs were ablated at time 0. Frame rate is 10 frames/s. In support of
800 Fig. 4.

Video 5. Sum of 6 z-slices from a time-lapse movie of stage 10A egg chamber expressing Par1::GFP (cyan) and Bazooka::mCherry (yellow). PFCs were ablated at time 0. Frame rate is 10 frames/s. In support of Suppl. Fig. 3.

Video 6. Sum of 6 z-slices from a time-lapse movie of stage 9 egg chamber expressing Par1::GFP (cyan) and *oskar::MS2*-mCherry (magenta). PFCs were ablated at time 0. Frame rate is 5 frames/s. In support of Fig. 5.

Video 7. Sum of 6 z-slices from a time-lapse movie of stage 9 egg chamber expressing microtubule marker Jupiter::GFP (green) and *oskar::MS2*-mCherry (magenta). PFCs were ablated at time 0. Frame rate is 5 frames/s. In support of Fig. 5.

Video 8. Sum of 6 z-slices from a time-lapse movie of egg chamber expressing Bazooka::mCherry (magenta) in the germline and aPKC::GFP (green). PFCs were ablated at time 0. Frame rate is 5 frames/s. In support of Fig. 6